TENSION WOOD ANATOMY OF SILVER MAPLE

by

Floyd George Manwiller

A Dissertation Submitted to the

Graduate Faculty in Partial Fulfillment of

The Requirements for the Degree of

DOCTOR OF PHILOSOPHY

Major Subjects: Wood Science
Plant Cytology

Approved:

In Charge of Major Work

Heads of Major Departments

Dean of Graduate College

Iowa State University
Of Science and Technology
Ames, Iowa

1966

TABLE OF CONTENTS

INTRODUCTION

Hardwood trees of many species contain an abnormal tissue called tension wood. This tissue, which forms on the upper side of branches and leaning stems, is characterized by fibers containing an internal unlignified gelatinous layer. Other layers of the cell wall may or may not have reduced lignification.

This abnormal tissue is of great economic importance because of its effect on many of the physical and mechanical properties of the wood. Tension wood tissue has excessive longitudinal shrinkage, and when it occurs in the same piece with normal tissue, differential shrinkage often causes warping and splitting. Tension wood also causes irreversible collapse in the wood during drying. Tension wood fibers have large numbers of slip planes and minute compression failures which give rise to many broken fibers upon acid maceration (Wardrop and Dadswell, 1947). The surfaces of sawn boards and veneer have a rough woolly appearance caused by tension wood tissue tearing loose in bundles of cells. These bundles can choke and overheat the saw in extreme concentrations. Tension wood is weaker than normal wood for most strength properties.

The explanation for the abnormal behavior of the tension wood tissue must ultimately be found in the chemical and physical organization of the cell wall. It was the objective of this study to determine the sequence, thickness, and fibril angle of cell wall layers in reaction wood tissue of silver maple (Acer saccharinum L.).

Silver maple was used for the study because of its increasing econ-

omic importance for furniture, core stock, and other exacting uses. It is a fast-growing bottomland tree which may increase as much as one-half inch in diameter per year and grows most rapidly during the first 50 years (U. S. Forest Service, 1965). In Iowa it is third in sawtimber volume, with only American elm and cottonwood ahead of it (Brendemuehl, et al., 1961).

Silver maple trees are phototropic and are therefore characterized by leaning stems which are often forked with large branches. Because of these growth patterns, tension wood is present in significant concentrations in the species (Arganbright, 1964) and is of considerable concern to commercial users.

REVIEW OF LITERATURE

In normal wood, longitudinal shrinkage from the green to the ovendry condition is approximately 0.1 to 0.3% (Koehler, 1960). Tension wood, however, has abnormally high longitudinal shrinkage, with values up to 1.55% (Baudendistel and Akins, 1946). There is a direct relationship between the concentration of gelatinous fibers and longitudinal shrinkage (Baudendistel and Akins, 1946; Pillow, 1950; Wahlgren, 1957). Terrell (1952) found that longitudinal shrinkage was only moderately related to the concentration of gelatinous fibers and that the relationship varied widely. Ollinmaa (1956) found that the rate of increase in shrinkage decreases as large amounts of tension wood are found.

Less information is available on the transverse shrinkage of tension wood. Several authors found that tangential shrinkage of tension wood was greater than that of normal wood, but radial shrinkage did not differ (Clarke, 1937; Rendle, 1937; Baudendistel and Akins, 1946; Dadswell and Wardrop, 1949; Onaka, 1949). Barefoot (1963) found that longitudinal shrinkage increased, while radial and tangential shrinkage decreased in wood containing gelatinous fibers. Arganbright (1964), working with soft maple, found that longitudinal shrinkage increased with increasing percent of gelatinous fibers, while radial and tangential shrinkage decreased.

Shrinkage in normal wood is a result of microfibril structure and orientation in the cell walls. The structural units of cell walls which can be observed with the electron microscope are called microfibrils.

They are extremely long and are composed of cellulose molecules. A cellulose molecule is a long, straight, unbranched chain of glucose units with numerous hydroxyl groups along its length. These hydroxyl groups are available for lateral bonding to other chains. As a result of these characteristics, the straight cellulose molecules of the microfibril are able to lie parallel to each other. In regions along their lengths they become tightly packed and highly oriented by means of intermolecular hydrogen bonding between hydroxyl groups. These highly ordered units, at least 600 angstrom units long, are termed crystallites. Between the crystallites are so-called amorphous regions where the cellulose molecules have a lower degree of order.

The microfibrils are helically wound about the cell longitudinal axis. They vary in their transverse dimensions depending on their source. Preston (1951) measured diameters up to 380 A in valonia. For wood cell walls Hodge and Wardrop (1950) found widths between 50 and 100 A. The view held by many at the present is that a microfibril is made up of smaller threads called elementary fibrils (Mühlethaler, 1965). The elementary fibrils average 35 A in width and are fasciculated to form the large microfibrils. Surrounding the crystalline core and separating adjacent microfibrils is the paracrystalline sheath, composed mainly of noncellulosic polysaccharides with a low degree of order. Lignin penetrates the non-crystalline areas.

Exposed hydroxyl groups of the cellulose, noncellulosic polysaccharides, and lignin bind polar water molecules by means of hydrogen bonding. Water molecules do not penetrate the tightly packed crystallites whose

hydroxyl groups are unavailable because of interchain bonding; only the
crystalline surfaces and the noncrystalline regions are involved in sorp-
tion of water. As water molecules move out of the wood during drying
the polysaccharide chains come together causing lateral shrinkage. There
is little shrinkage in the axial direction, however, since this is the
direction of orientation of the long cellulose chains (Cockrell, 1946;
Peck, 1957; Koehler, 1960).

It can be seen that there is shrinkage between microfibrils but
little along their length. The wall of a typical fiber from a nonleaning
tree is made up of the primary wall and the secondary wall, which con-
sists of three layers: the S_1, S_2, and S_3 layers (Figure 1). On the
lumen side of the secondary wall is formed the warty layer. The follow-
ing description of typical walls is taken from Panshin, DeZeeuw and Brown
(1964) and Wardrop (1964). The primary wall is about 0.1 micron thick in
the green condition. The microfibrils are considerably dispersed with an
approximately transverse orientation on the inner surface and a random
one with a tendency to transverse on the outer surface. Most of the micro-
fibrils have a fibril angle (the angle formed by the microfibril and the
longitudinal axis of the cell, see Figure 1) of 75 to 90°. There is no
lamellation in the primary wall.

The outer layer, the S_1, of the secondary wall is about 0.1 to 0.2
micron thick and is composed of some four lamellae of alternately crossed
microfibrils. If, in the lamella wall nearest the observer, the micro-
fibrils spiral upward to the right, the helix is termed a Z helix, and
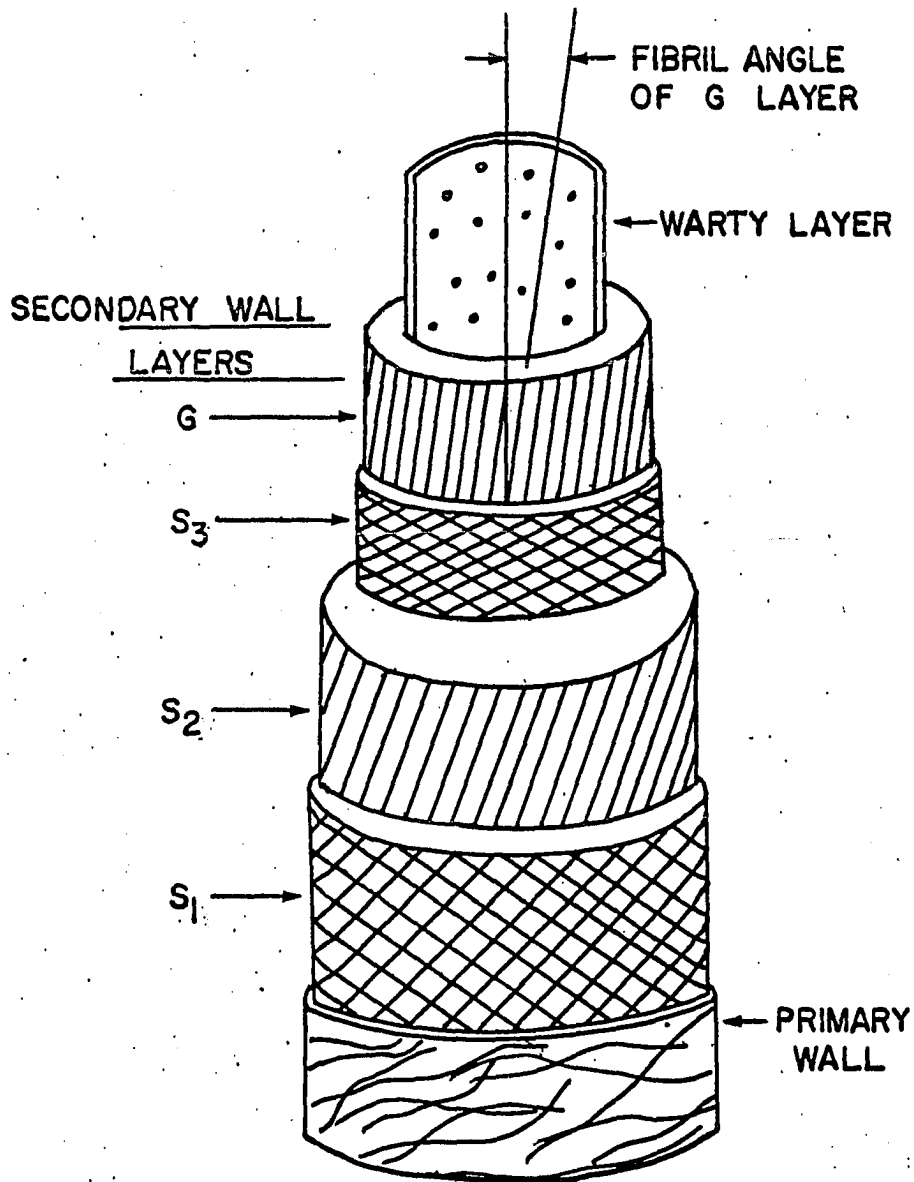if upward to the left, an S helix. The fibril angle of the S_1 lamellae

Figure 1. Cell wall of a hardwood fiber, with all possible layers depicted

is 40 to 55°.

The middle or S$_2$ layer is the thickest of the wall layers and constitutes the bulk of the cell wall. It consists of numerous concentric lamellae of uniform fibril angle. The fibril angle is 10 to 30°, and the helix usually has a Z orientation.

The inner layer, the S$_3$, appears to be thinner than the S$_1$ layer, with several lamellae of alternating S and Z helices. The microfibrils are not as well oriented, however, as those of the S$_1$. The fibril angle is typically 60 to 90°.

On the lumen side of the S$_3$ layer is often found the warty layer. It is present in the tracheids, fibers, and vessels of most species. This layer is also found in tension wood cells (Liese, 1965). The warty layer consists of two amorphous membranes with spherical particles, the warts, lodged between them. Liese (1965) has found that the average diameter of the warts lies between 0.1 and 0.25 micron. Little is known about the chemical composition of the warty membrane, but the presence of protein is indicated in the warts themselves since they--but not the membranes--absorb ultraviolet light, and the warts give a positive reaction with methylene blue. It is hypothesized that the outer layer represents the plasmalemma and the inner layer, the tonoplast. The electron-dense warts are formed in the cytoplasm during the latter stages of aging, but their origin is not known (Liese, 1965). On the death of the cell the two membranes, with the warts between, collapse onto the cell wall.

It is clear that the dominant S$_2$ layer controls shrinkage in normal wood. With the exception of the amorphous warty layer, each of the layers

other than the S_2 would by itself have a large shrinkage component in the longitudinal direction of the wood. Longitudinal shrinkage therefore increases as the fibril angle of the S_2 layer increases (Koehler, 1960).

The extent to which the anatomy of the tissue of leaning trees is modified varies greatly. In some genera such as Fraxinus (Clarke, 1937) and Tilia (Onaka, 1949) there is no modification in anatomy. In some cases there is reduced cell wall lignification in zones where tension wood might have been expected. This has been termed "incipient tension wood" (Dadswell and Wardrop, 1956).

A few studies have revealed variations from what is considered typical tension wood described below. Using staining techniques, Jutte (1956) found that the secondary wall of various fibers of wane (Ocotea rubra) contained two to four layers which were alternately lignified and unlignified. Wahlgren (1957) found the same organization for Quercus lyrata.

In the many species containing typical tension wood the anatomical modifications are great. In these species the vessels are fewer and smaller than in normal wood (Chow, 1946; Onaka, 1949). The parenchyma and rays are unmodified. Anatomical variations are also evident in the wall structure of the fibers. These modified fibers, called gelatinous fibers, contain a secondary wall layer termed the gelatinous (G) layer (Figure 1). Gelatinous fibers may appear in bands or scattered individually or in small groups among apparently normal fibers. They are most heavily concentrated in the early wood.

The G layer may replace one or more of the secondary wall layers

or be present in addition to them. The primary wall is always present. Onaka (1949) and Wardrop and Dadswell (1955) have found the following variations in the secondary wall layering sequence:

(a) S_1, G

(b) S_1, S_2, G

(c) S_1, S_2, S_3, G

Onaka stated that tension wood of each hardwood family is characterized by a specific layering sequence. He classified Aceraceae as of type (c). Wardrop and Dadswell (1955), however, found type (a) in the early wood of Eucalyptus gigantea and type (b) in the late wood in the same specimen.

The gelatinous layer is highly crystalline and unlignified and is poorly bound to the rest of the cell wall. The thickness of the G layer is quite variable, and in extreme tension wood formation may almost fill the lumen (Wardrop and Dadswell, 1948).

The structure of the cell wall layers other than the G layer appears to be similar to that of normal fibers. Wardrop and Dadswell (1948), based on X-ray, polarizing microscope, and visual observations, conclude that the S_1 and S_2 layers of gelatinous fibers have a steeper spiral orientation than do those of normal wood. The S_1 layer often appears thinner than in normal fibers, especially in those in which the layering sequence is P + S_1 + G. In the electron microscope the S_1 shows the usual lamellation; the variation in thickness evidently is the result of variation in the number of lamellae present (Wardrop, 1964). Wardrop and Dadswell (1948) found that the S_1 in transverse section has lower birefringence. Dadswell (1964), referring to this work, states that it

is not known whether this reflects a difference in fibril angle or in composition.

Preston and Ranganathan (1947), using X-ray diffraction, found the fibril orientation of the G layer to be nearly axial. Wardrop and Dadswell (1948, 1955) confirmed this by determining the major extinction position of macerated tissue using a polarizing microscope. In the earlier publication they report a fibril angle of 5° to 8°. Wardrop and Dadswell (1955) and Côté and Day (1962) also found an approximately axial orientation in electron microscope studies.

Electron microscope studies of the G layer have added to the knowledge of its structure. Casperson (1961) found the G layer of Aesculus hippocastanum to consist of concentric lamellae (10 in the mature cell) with possible "bridges" between lamellae to give a honeycomb effect. Côté and Day (1962) described the G layer as being parallel lamellar or mesh-like. They were able to identify individual microfibrils roughly circular in cross section and 200 to 400 A in diameter. Sachsse (1962, 1963), working with Populus X regenerata, observed that the G layer has a honeycomb structure with the lamellae joined through bond points. Côté and Day (1962) and Sachsse (1962, 1963) report a thin lamella similar to the S_3 on the lumen side of the G layer.

Wardrop and Dadswell (1948) found that the extent of hydrolysis in a given time was less for tension wood than for normal wood and felt that this indicated a higher degree of crystallinity in the tension wood cellulose. They found in a later study (Wardrop and Dadswell, 1955) that

tension wood has a lower equilibrium moisture content and sharper X-ray diffraction diagrams. Using benzene as a displacement liquid they found that tension wood has a higher density of cell wall substance. These factors all indicate a higher degree of crystallinity than in normal wood. They also found by X-ray diffraction that the crystallites in the micro-fibrils of tension wood are wider than in normal wood, but that the par-acrystalline phases are of similar size. Chow (1946) found that tension wood had a higher cellulose content and lower pentosan content.

The G layer undergoes extreme and largely irreversible shrinkage upon the loss of water (Wardrop and Dadswell, 1948, 1955). Wardrop (1964) therefore feels that the microfibrils must be relatively widely separated from each other in the green condition. Based on his observations with the electron microscope he feels that they are uniformly distributed. Côté and Day (1962) found that when tension wood specimens are embedded in methacrylate for ultrathin sectioning, the G layer expands but the rest of the wall does not. They interpret this to mean that there is relatively weak lateral bonding and a lack of encrusting materials in the G layer.

The G layer, then, is more highly crystalline than normal wood, and the almost axial fibril angle is much steeper than that of any of the other wall layers. It would appear that whether the gelatinous layer was present as an extra layer or replaced the S_3, the S_2, or both it would result in even less longitudinal shrinkage. As has been described above, however, the opposite is true, and the cause of this abnormal longitudinal shrink-age is unknown.

EXPERIMENTAL INVESTIGATION

General Considerations

As was discussed in the literature review, shrinkage occurs primarily at right angles to the long axis of the microfibrils. The microfibril orientation in the wall layers then determines the shrinkage anisotropy of the cell. The loss of a wall layer or a change in its thickness or microfibril orientation could affect the shrinkage pattern of the cell. Barefoot (1963) hypothesized that a change in fibril angle could explain his shrinkage results.

The literature reveals that, in general, an increase in the concentration of gelatinous fibers causes increased longitudinal shrinkage during drying. This increased shrinkage may be simply a greater concentration of anatomically similar gelatinous fibers. It is also possible that the stimulus to greater gelatinous fiber production may also accentuate the anatomical modifications of the cells of the reaction wood zone.

Arganbright (1964), studying soft maple, found that samples from the reaction wood zone of a tree leaning 10° had an average longitudinal shrinkage of 0.877 percent. Samples from this zone in a tree leaning 28° had an average longitudinal shrinkage of 1.001 percent. Within the reaction wood zone of the 10° tree longitudinal shrinkage increased with increasing gelatinous fiber percentage while in the 28° tree there was no such relationship. This suggests differences in the reaction wood zones of the two trees.

Objectives

One objective was to develop the technique for measuring the fibril angle within individual layers of the cell wall and to develop a statistical approach for comparing the values obtained.

The specific objective of this study was to determine, through use of the polarizing microscope: (1) the layering sequence, (2) layer thickness, and (3) layer fibril angle in the radial cell walls of both normal wood and tension wood of silver maple. Specifically, normal fibers from a non-leaning tree were compared with fibers (both gelatinous and non-gelatinous) from the tension wood zone of trees having 10- and 20- degree lean. The electron microscope was used to verify these observations and to observe the fine structure of the G layer.

Polarizing Techniques

A crystalline solid is composed of ions, atoms, or molecules which are present in a highly ordered three-dimensional repetitive pattern. The various properties of such a solid are different in different directions and the solid is said to be anisotropic. Other solids are composed of randomly arranged units. These amorphous solids and liquids are isotropic.

Wood has anisotropic properties because in the cell wall layers both the microfibrils and the cellulose molecules of which they are composed have an ordered repetitive arrangement.

Light is a form of radiant energy whose optical properties are explainable by the electrical vector of the electromagnetic theory. Light

travels in continuous waves varying in time and place according to the
sine law. The waves vibrate at right angles to the direction of pro-
pagation. The color of the light is determined by the wave length, and
the amplitude determines the intensity.

A beam of light if viewed along its direction of propagation, will
have vibrations in all planes. The polarizing microscope is optically
similar to simple compound microscopes except that it contains a pol-
arizer below the condenser and an analyzer between the objective and the
eyepiece. These elements are crystals that transmit light vibrating in
one plane only. When the vibration directions of the polarizer and an-
alyzer are at right angles to each other, no light reaches the observer.

Plane-polarized light from the polarizer passes through isotropic
materials optically unchanged. In uniaxial anisotropic materials such
as wood, it travels unchanged in one direction only--the optic axis,
which is parallel to the longitudinal axis of the microfibril. In any
direction other than parallel to the optic axis the incident plane-
polarized light is split into two rays vibrating in mutually perpen-
dicular directions. Light now reaches the observer through the crossed
analyzer with the maximum brightness being obtained when the vibration
directions of the specimen are at 45° to those of the crossed polarizer
and analyzer (Figure 2).

These optical phenomena can be used to identify the cell wall layers.
When a transverse section of wood is viewed between crossed polarizer
and analyzer, the isotropic intercellular substance appears dark. The
primary and S_1 layers both appear bright (and indistinguishable from

ANALYZER
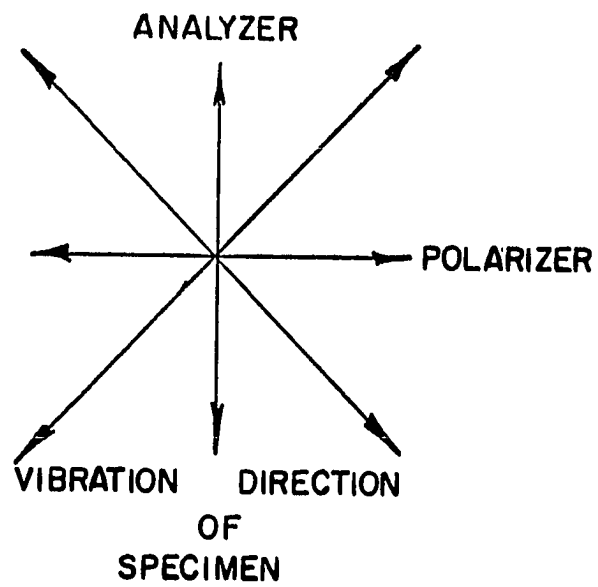
POLARIZER

VIBRATION   DIRECTION
OF
SPECIMEN

Figure 2.   Orientation of specimen with respect to polarizer and
analyzer in polarizing microscope

each other) since they are viewed at a great angle to their respective optic axes. The S_2 layer is much darker since it is viewed more nearly parallel to the optic axes of its microfibrils. On the lumen side of the S_2 is the adjacent bright S_3. Finally, the G layer, if present, appears dark.

Preston (1952) has developed a technique for measuring the steepness (fibril angle) and direction of winding of the helix within any one wall layer. The technique, using a polarizing microscope equipped with a Senarmont compensator, has not been explained in detail in print. The following explanation is based on the books by Johannsen (1918), Preston (1952), and Wahlstrom (1960), and the Zeiss Senarmont Compensator instructions (Carl Zeiss, ca. 1956).

The interaction of light and matter can be expressed by the index of refraction (n), which can be calculated (among other ways) by dividing the velocity of light in air by its velocity in the material. The difference between the refractive indices of the perpendicular rays is referred to as the birefringence. One of the rays, termed the ordinary or O ray, vibrates at right angles to the optic axis regardless of how the incident light strikes the specimen, and its refractive index (n_0) has a constant value. The other ray, the extraordinary or E ray, vibrates in the plane of the optic axis and at an angle to it, depending on the angle at which the incident beam strikes the specimen. Its refractive index (n_E) varies, and reaches its maximum in wood when the incident light is perpendicular to the optic axis. The incident light is then also perpendicular to the longitudinal axis of the microfibrils, and the bire-

fringence ($n_E - n_0$) is maximum.

In a cell wall layer, shown in Figure 3, where the microfibrils are wound in a Z helix, if sections were cut along planes A, B, and C, and birefringence values were measured in the wall that is nearest the observer, section B would have the highest birefringence since it is parallel to the orientation of the microfibrils. If the angle which each section makes with the fiber's longitudinal axis is measured and the birefringence plotted against that angle, a curve is obtained. The curve's peak, the maximum birefringence, indicates the angle of the section parallel to the fibrillar orientation and therefore the fibril angle.

Whether a cell wall layer has a Z or S helix may be determined by plotting birefringence against section angle for two opposing walls. If a layer contains a Z helix as in Figure 3, the birefringence curve will have a peak in the near wall but none in the back wall because there, none of the sections would be parallel with the microfibrils. If the microfibrils were wound in an S helix, the curve of birefringence against section angle would have a peak in the far wall and none in the near wall. The S_1 and S_3 layers, with alternating lamellae of S and Z helices, should produce curves with peaks from both walls.

The Senarmont compensator converts elliptical vibration to linear. With the linearly polarized light it is possible to measure the phase difference between the two rays, and from this, to calculate the birefringence. The measurement must be made in monochromatic light of the
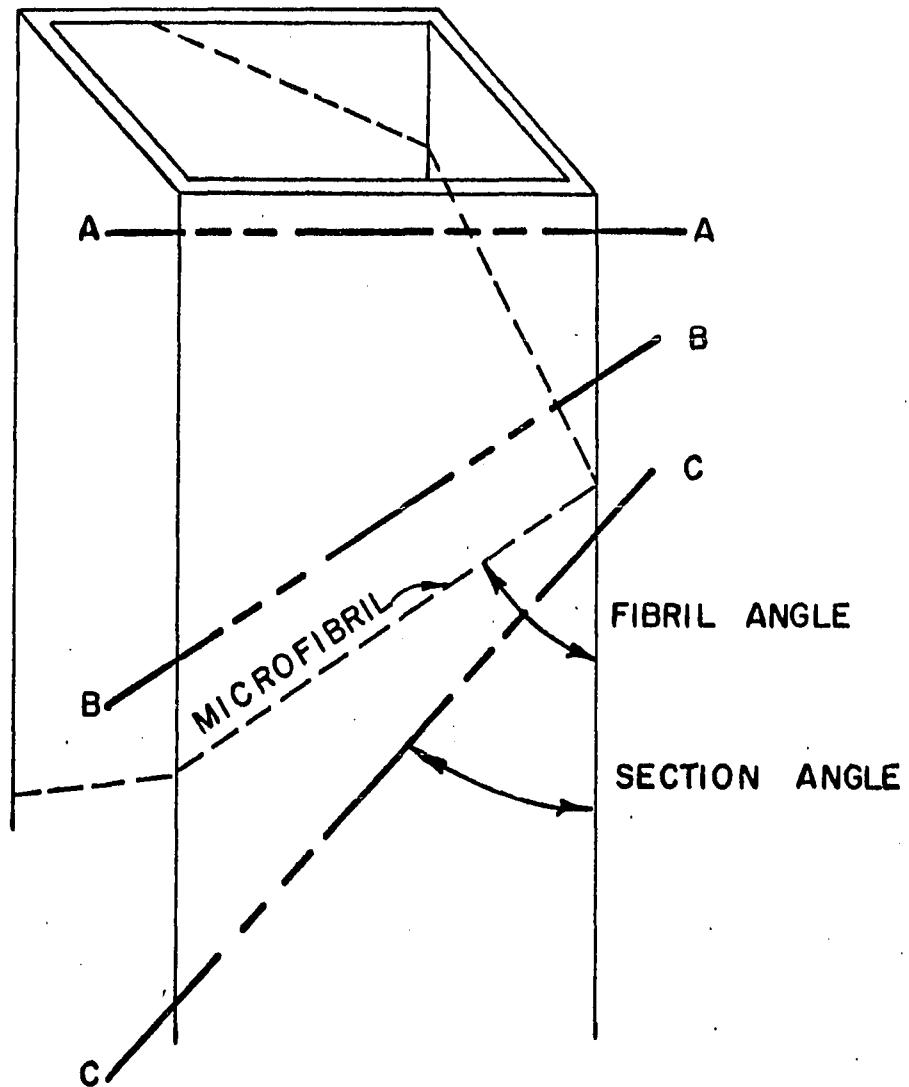
Figure 3. Cell wall layer with microfibrils in a Z helix

wavelength for which the compensator is designed.

The polarizer and analyzer are crossed in the microscope to give extinction, and the specimen is oriented with its directions of vibration at 45° to those of the polarizer and analyzer (Figure 2).

The light waves, which are plane-polarized upon leaving the polarizer, are divided by the specimen into two mutually perpendicular rays of equal amplitude. They acquire a phase difference by passing through the specimen. The magnitude of the difference depends on the difference in refractive index and thickness. Upon emerging from the specimen, the two rays interfere to produce elliptically polarized light (as depicted by A, B, and E, Figure 4). The ellipse axes a and b are 45° to the vibration directions of the specimen and therefore parallel and perpendicular, respectively, to the polarizer direction. The ellipse dimensions depend on the difference in phase between the two rays. To measure the phase difference the elliptical light is converted back to plane-polarized light. The vibration direction of the plane-polarized light is determined by the vectors of the two emerging rays. The angle of rotation required to bring the analyzer back to extinction is a measure of the phase difference.

The same elliptical vibration would have resulted from two rays that differ from each other in amplitudes of a/2 and b/2 and have a constant phase difference of 90° (C, D, and E, Figure 4). A plane-polarized vibration results when two rays differ in phase by 0 or 180 degrees. If the elliptical vibration is considered to be formed by the components with a phase difference of 90°, it can be transformed
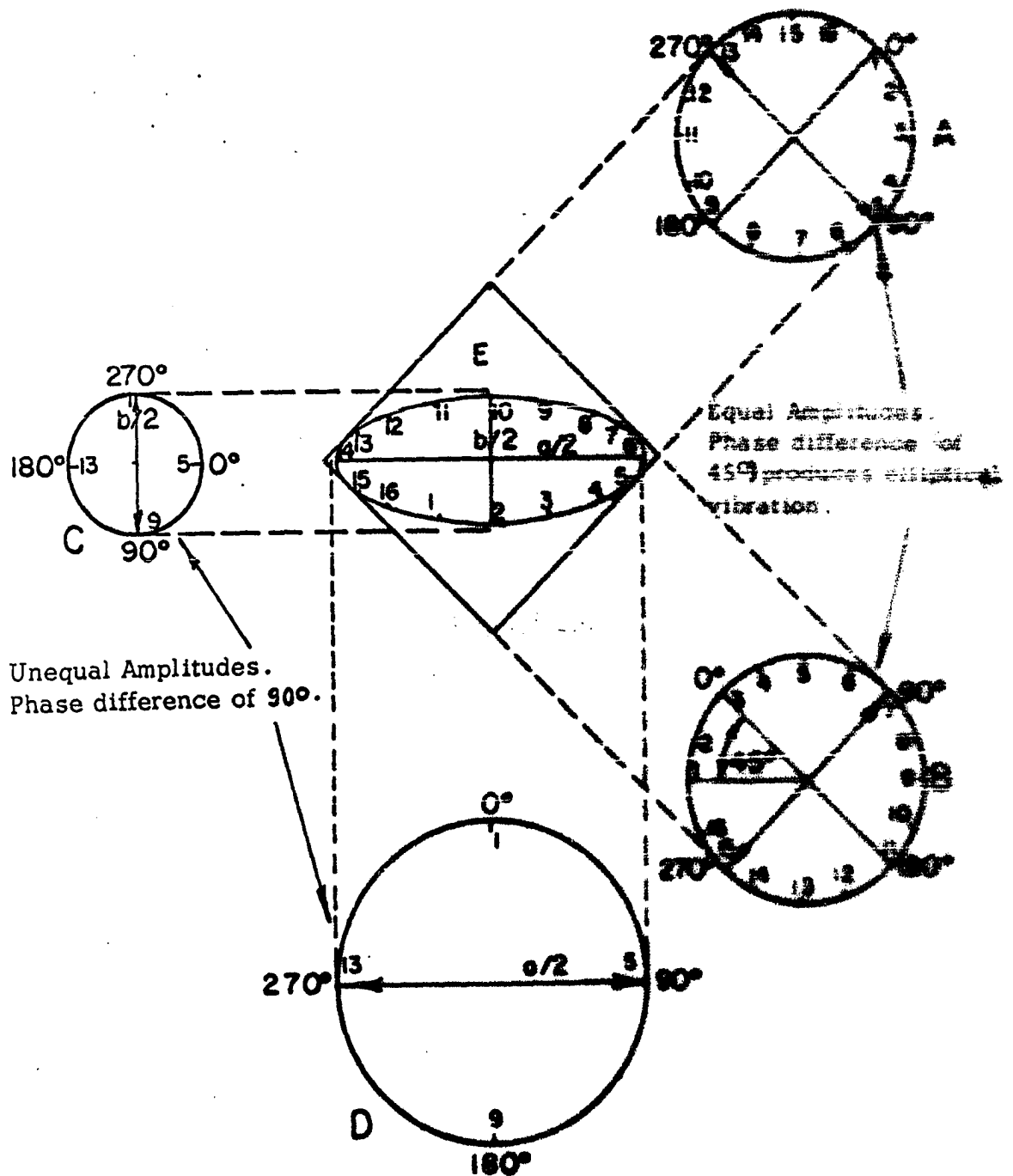
Figure 4. Production of the same ellipse by two rays of equal amplitudes and intermediate phase difference or by two rays of unequal amplitudes (a/2 and b/2) and phase difference of 90°
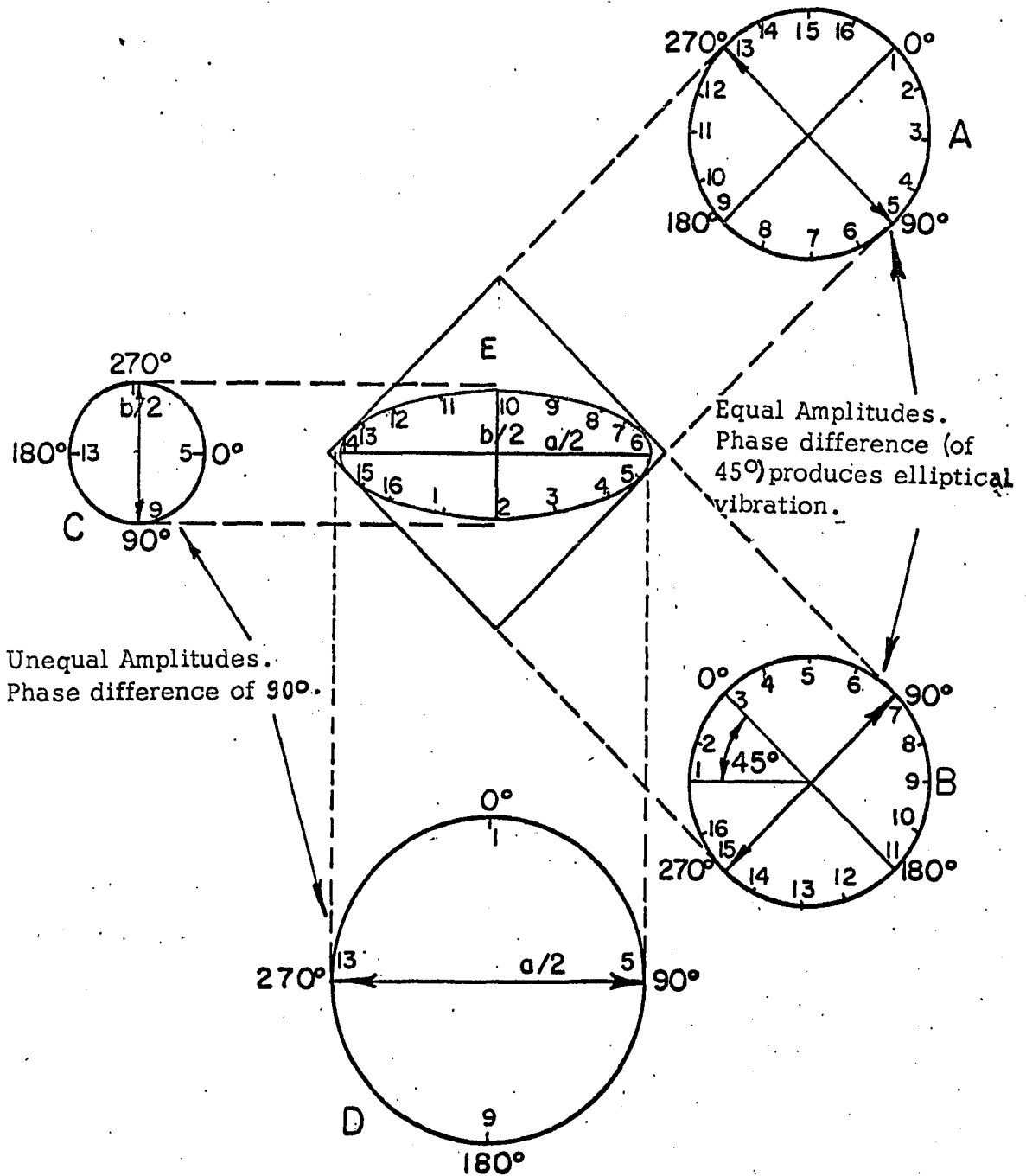
Figure 4. Production of the same ellipse by two rays of equal amplitudes and intermediate phase difference or by two rays of unequal amplitudes (a/2 and b/2) and phase difference of 90°

into a linear vibration by adding or subtracting a phase difference of

90° to produce the required difference of 0 or 180°.

The Senarmont compensator, a quarter-wave plate, makes a phase change

of 90°. When its vibration directions are aligned with those of the

elliptical light produced by the specimen, it separates the light into

two rays of a/2 and b/2 amplitude with a phase difference of 90° (C, D,

Figure 4) and then either increases or decreases this difference by 90°.

If the slow (extraordinary) ray of the specimen is positioned 45° counter-

clockwise from the slow ray of the compensator (Figure 5), the slow ray

of the ellipse formed will be aligned with the fast (ordinary) ray of the

compensator and will be speeded up; at the same time the fast ray of the

ellipse will be lined up with the slow ray of the compensator and there-

fore slowed down. The net effect is to reduce to 0 the original ellipse

phase difference of 90°. The light emerging from the compensator is

then linear and passes through quadrants I and III (Figure 6). The

analyzer would be rotated counterclockwise through an angle of ϕ to

reach extinction.

If the slow component of the specimen is positioned 45° clockwise

(Figure 7) from the slow ray of the compensator, the fast and slow rays

of the ellipse formed will be aligned with the corresponding rays of the

compensator. The ellipse slow ray will then be slowed and the fast ray

speeded up. The phase difference is then increased from 90 to 180°, with

the resulting linear vibration passing through quadrants II and IV

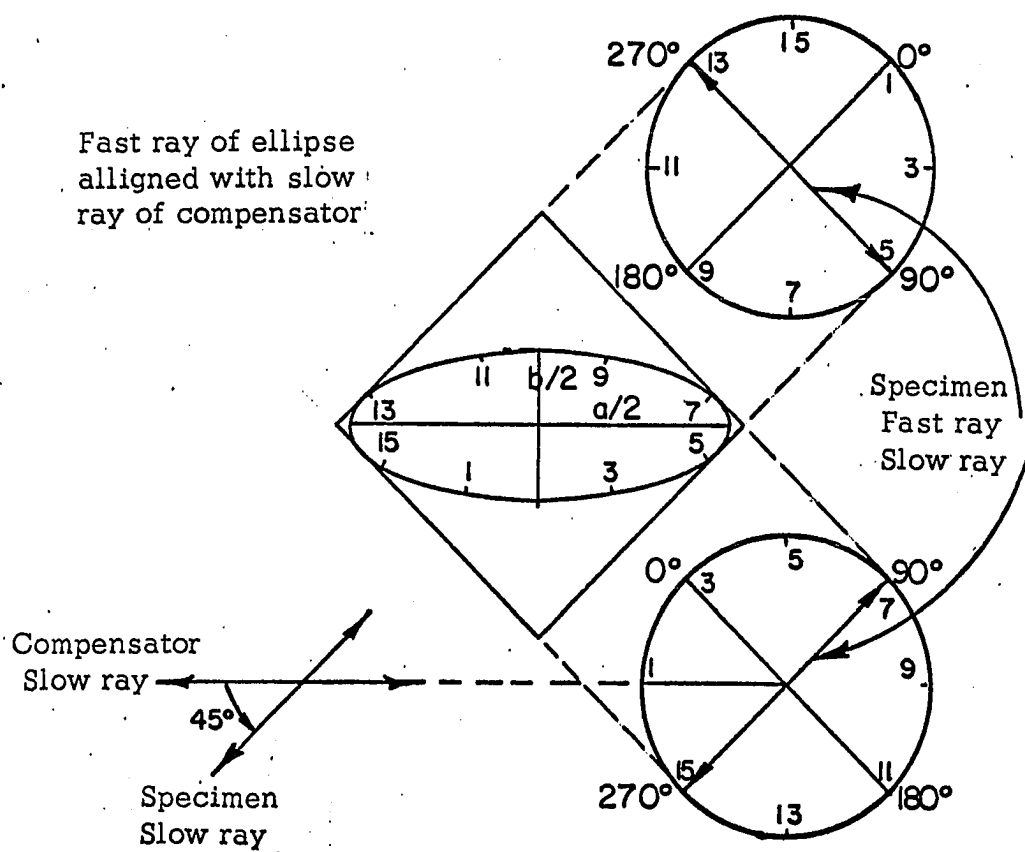(Figure 8). The analyzer would be rotated clockwise through ϕ to reach

extinction.

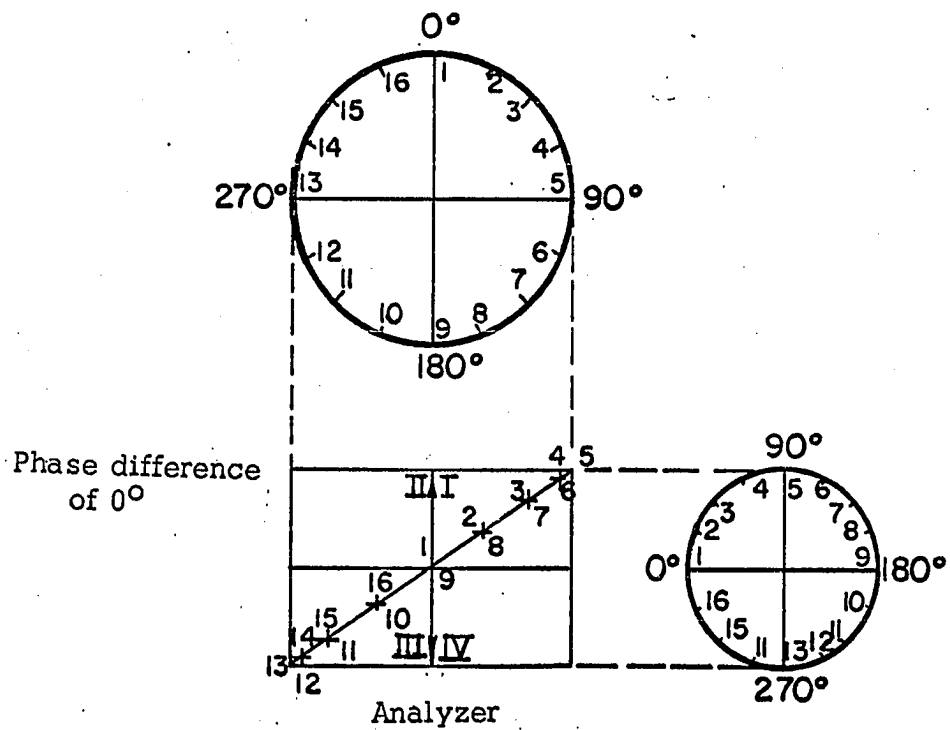Figure 5. Specimen oriented with slow ray 45° counterclockwise from that of compensator

Figure 6. Orentation of the linear vibration when Senarmont compensator has reduced 90° phase difference to zero. Analyzer would be rotated counterclockwise to reach extinction

As mentioned earlier, the retardation of one ray with respect to the other depends on wave velocities and section thickness. The velocities are dependent on the refractive indices n_E and n_0, respectively.

Let t_E be the time for the slow ray to pass through the section and t_0 the time for the fast ray. Then if d is the thickness,
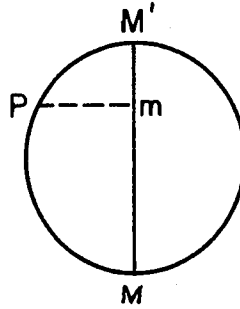
$$t_E = n_E d$$

$$t_0 = n_0 d$$

and the retardation = $t_E - t_0 = d(n_E - n_0)$, often referred to as the path difference.

We are interested in determining the birefringence, $n_E - n_0$, and, as stated above, the Senarmont compensator measures the phase difference.

The path difference is related to the phase difference in the following manner:

The point m is vibrating along M M' with simple harmonic motion. Point P is located on a circle with diameter of M M'. P m is perpendicular to M M'. When P travels around the circle with constant velocity, m moves along M M'. When point m moves from M to M' and back again, one vibration has been completed, i.e., one path length of λ. During the same time point P makes one complete revolution, passing through 2π radians. Thus, a path difference of λ = a phase dif-
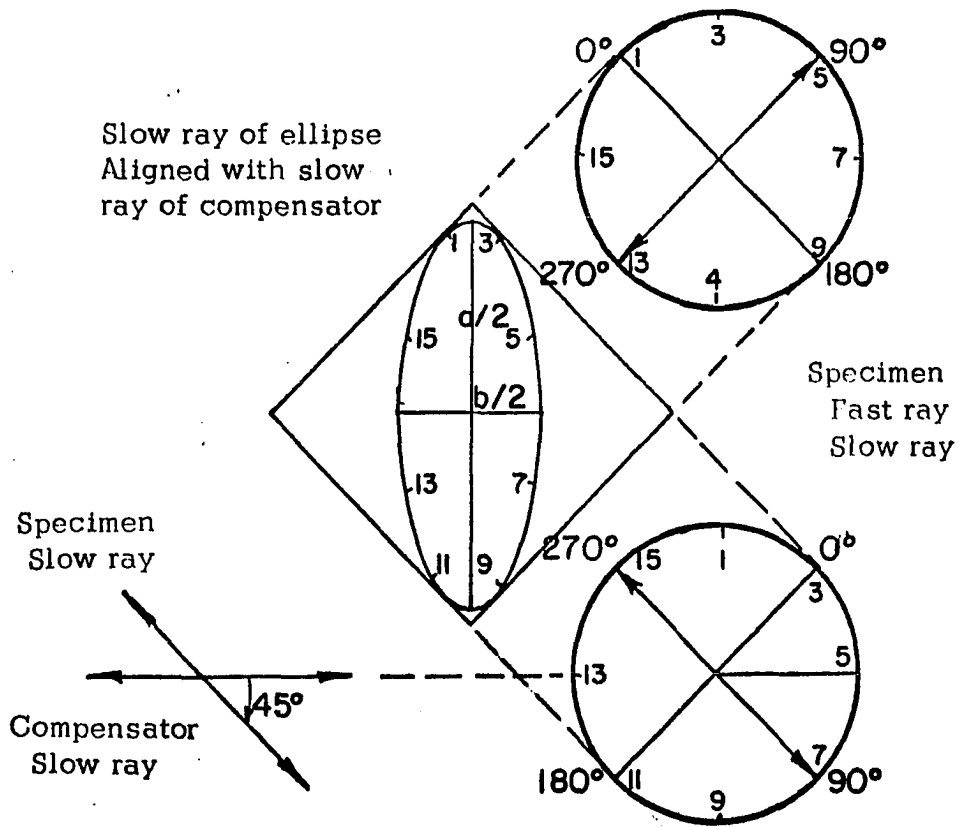
Figure 7. Specimen oriented with slow ray 45° clockwise from that of compensator. Slow ray of ellipse produced is parallel to that of compensator.
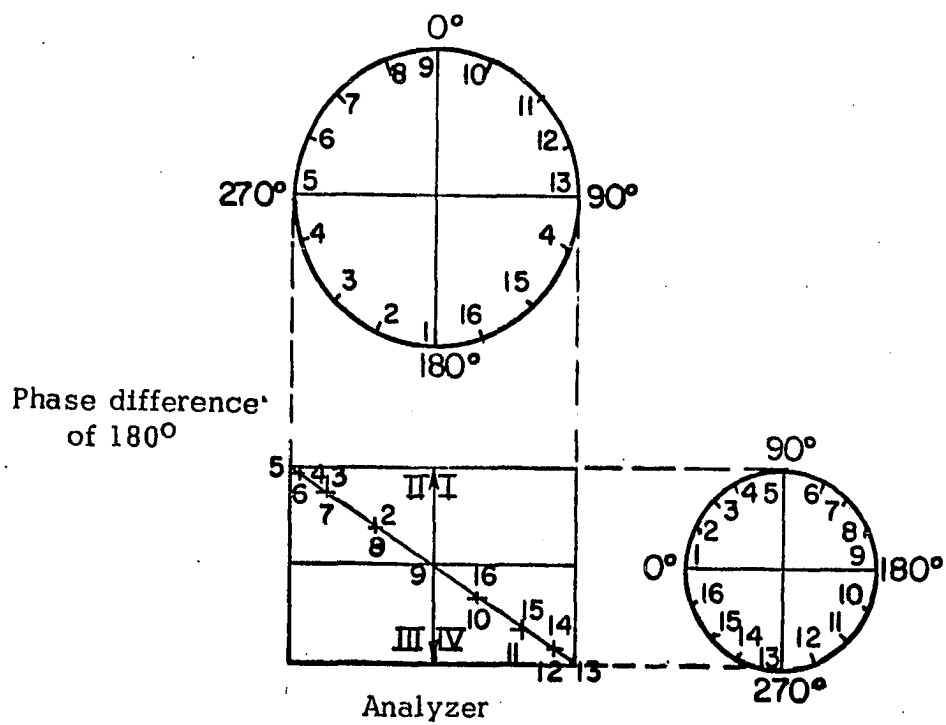
Figure 8. Orentation of linear vibration when compensator has increased 90° phase difference to 180°. Analyzer would be rotated clockwise to extinction

ference of 2π , and a path difference of $(n_E - n_0)d$ = a phase differ-

ence of $(n_E - n_0)$ (d) $\dfrac{2\pi}{\lambda}$, where d is the thickness of the section.

The rotation of the analyzer to extinction, ϕ, equals half the phase

difference. Extinction occurs when the path difference is $\lambda/2$, $3\lambda/2$.

$5\lambda/2$, etc. -- every 1λ or every 360°. But in the microscope extinc-

tion occurs whenever the analyzer is perpendicular to the linear vibra-

tion, or twice in a rotation. Therefore 180° of analyzer rotation equals

360°, or ϕ equals half the phase difference.

Therefore, referring back to the above equation, $2\phi = (n_E - n_0)$

(d) $\dfrac{2\pi}{\lambda}$, and the birefringence $n_E - n_0 = \dfrac{\phi\lambda}{\pi d}$. λ and d are

in microns. Therefore,
$$n_E - n_0 = \frac{(\phi \text{ degrees})\ (\lambda \text{ microns})}{(3.1416 \text{ radians})(57.2956 \text{ deg/rad})(d \text{ microns})}.$$

Procedure

During the winter of 1964-65 samples were taken from three silver

maple trees. One tree was straight and non-leaning, one leaned 10° from

the vertical at breast height, and the third leaned 20° at breast height.

Environmental factors were assumed to be constant since the trees were

growing together on the same aspect, were all about 45 years old and of

the same size, and had approximately the same position in the crown cover.

A single specimen was taken at breast height from each tree. The

sample was taken from the upper side of the leaning trees; in the non-

leaning tree it was taken at random. Sample dimensions were approx-

imately 10 cm longitudinally, 5 cm tangentially, and 2 cm radially. Each

block was removed by boring holes around its outline and splitting it

free with a chisel. The top of each block was notched on removal to

record its orientation in the tree. The block was then immediately submerged in water and stored in a refrigerator until used.

Preparatory to sectioning, each large block was reduced to several small ones measuring approximately 6 mm tangentially and the original 10 cm longitudinally. Radially they included the 1962, 1963, and 1964 growth rings. Measurements were made only on the ring for 1963, a year of normal growth. Further, the observations were confined to the earliest formed one-fourth of the ring to avoid the inherent variation across the ring. A corner (the same one each time) was removed from each block by making a full-length longitudinal bevel cut. The orientation in the tree of each subsequent microtome section was indicated by the missing corner. The 10-cm-long blocks were reduced to a series of microtome blocks that were approximately 5 mm thick with radial and tangential dimensions described above. The sectioning surfaces of the series of blocks varied from transverse to longitudinal in approximately 10° increments, i.e., there were about 10 blocks for each tree sampled. The series of sections from the blocks were the basis for the birefringence curves from which layer fibril angles could be determined. Since the birefringence measurements were to be made on the radial walls, the section angle desired was roughly indicated on the radial face using a protractor. A coping saw was used to cut away the waste material.

In polarizing microscopy thick or damaged sections cause light scattering which causes light layers to appear wider at the expense of dark ones. To make it possible to cut sections less than 10 microns thick and with the G layer relatively intact, the blocks were softened

and embedded (Carlson, ca. 1964). Softening was accomplished by boiling 1-1/4 hours in 1 part glacial acetic acid to 4 parts 3-percent hydrogen peroxide, followed by a 4-hour wash in tap water. The saturated blocks were embedded at 55°C. in polyethylene glycol to stabilize the green dimension (first in PEG 1000 for 4 hours, then in PEG 1540 for 4 hours). A vacuum was pulled periodically to increase penetration. The specimens were then placed in aluminum foil containers (boats) with fresh PEG 1540 and allowed to harden. These embedded blocks were then block-mounted and sectioned on a sliding microtome.

After the desired sections had been cut from each block, a thin longitudinal section was removed from the block's radial face with a razor blade. On this latter section it was possible to accurately measure the angle of sectioning with respect to the longitudinal axis of the cells. Ten determinations were made on each longitudinal section with a microscope equipped with an eyepiece for measuring angles.

A section from each microtome block in the series was mounted unstained in water, which dissolved the polyethylene glycol. Birefringence measurements were made on 20 cells in each section from the non-leaning tree, and 20 non-gelatinous and 20 gelatinous fibers in each section from the two leaning trees.

In the radial wall of each cell measured, a birefringence determination was made on each secondary wall layer (at 1000X). The wavelength used was 0.546 micron. It was obtained by using a filter with the regular tungsten light source. The birefringence equation is then:

$$\text{Birefringence} = \frac{\phi (0.003033)}{d}$$

where ϕ is the amount of analyzer rotation, in degrees, required for the cell wall layer to become dark, and d is the section thickness in microns.

After the analyzer rotation values were obtained, the section thickness was measured. The section was stained with hemalum (see Appendix) and the 1962 and 1964 growth rings were removed. The 1963 ring was infiltrated with PEG 1540 at 55°C. for 10 minutes and then placed in an aluminum foil boat with fresh PEG 1540 which was allowed to harden. The section was resectioned with a razor blade and 10 thickness measurements were made using a microscope equipped with a filar eyepiece micrometer.

Since the individual layers are visible in polarized light, their thicknesses were measured on transverse sections with an eyepiece filar micrometer. The thickness values obtained do not necessarily represent the true layer thicknesses since in the polarizing microscope one sees only the optical effects of the different fibrillar orientations. It was believed, however, that if only thin, good sections were used to reduce light scattering, and measuring was carefully done, valid comparisons could be made, and the thicknesses obtained would approach the true values.

The relative proportion of gelatinous to non-gelatinous fibers was determined for the leaning trees. Five microtome blocks from each tree were sectioned green prior to softening. The sections were stained with chloriodide of zinc (see Appendix) to differentially stain and swell the unlignified G layer for easier identification. Each section was projected at 430X by an overhead carbon arc projector onto a grid (Figure 9) developed by Arganbright (1964). Three grids were used for the 1964

growth ring in each section: one each for the early, middle, and late

portion of the ring. Thus 15 grids were used to obtain an indication of

the concentration of gelatinous fibers in the 1964 growth ring of each

leaning tree. In each of the 5 squares on a grid the total number of

gelatinous fibers and of non-gelatinous fibers was counted and then values

for the grids were totaled.

Specimens for electron microscopy were obtained by sectioning green

specimens at 80-120 microns on the sliding microtome. The sections

were reduced to smaller sizes of 0.5 to 1.0 mm on a side with a razor

blade. These small specimens were embedded in a mixture of 8 n-butyl

to 2 methyl methacrylate (see Appendix). Methacrylate was used as the

embedding medium because during polymerization it causes the G layer to

swell, revealing its internal structure.

GELATINOUS FIBER COUNT SHEET

TREE NO. _____

REGION   SP._____, MID._____, SU._____
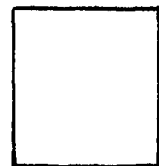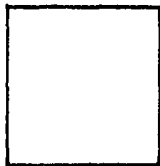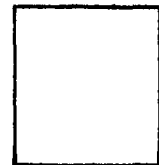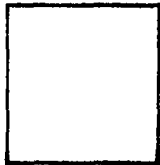
TOTAL NO. CELLS _____
TOTAL NO. GEL. FBRS. _____
PERCENT GEL. FBRS. _____

Figure 9. Grid used for determining the concentration of gelatinous
fibers in microtome sections (Arganbright, 1964)

RESULTS

Silver maple is a diffuse porous wood with the growth rings de-
lineated by a narrow, darker line of denser fibrous tissue. In the
trees studied, this band was up to 8 cells wide. An attempt was made
to make fibril angle determinations in this cell type, but the cells
proved to be libriform fibers which contain simple pits. The micro-
fibril orientation was highly deviated by the heavy pitting (Figure 10)
and birefringence curves could not be obtained. The S_3 layer of the
libriform fibers usually appeared to be missing or poorly developed.

The tree leaning 20° contained greater concentrations of gel-
atinous fibers than did the 10° tree, and these fibers differed from
those of the 10° tree in layering sequence, fibril angles, and some
layer thicknesses. Both gelatinous and non-gelatinous fibers of both
trees had a thinner S_3 layer (when present) with a greater fibril angle
than did the normal fibers.

The 10° tree contained 18-percent gelatinous fibers and the 20°
tree 48.5 percent. This was expected since Berlyn (1961) found that in
cottonwood there is a positive correlation between the degree of lean
and the amount of tension wood formed.

The G layer in specimens from both leaning trees showed the honey-
comb structure observed by Casperson (1961), Côté and Day (1962), and
Sachsse (1962), (1963), and the thin terminal lamella observed by the
latter researchers (Figure 11). Figure 12 indicates that the microfibrils
are common to more than one lamella. No warty layer was apparent in ob-
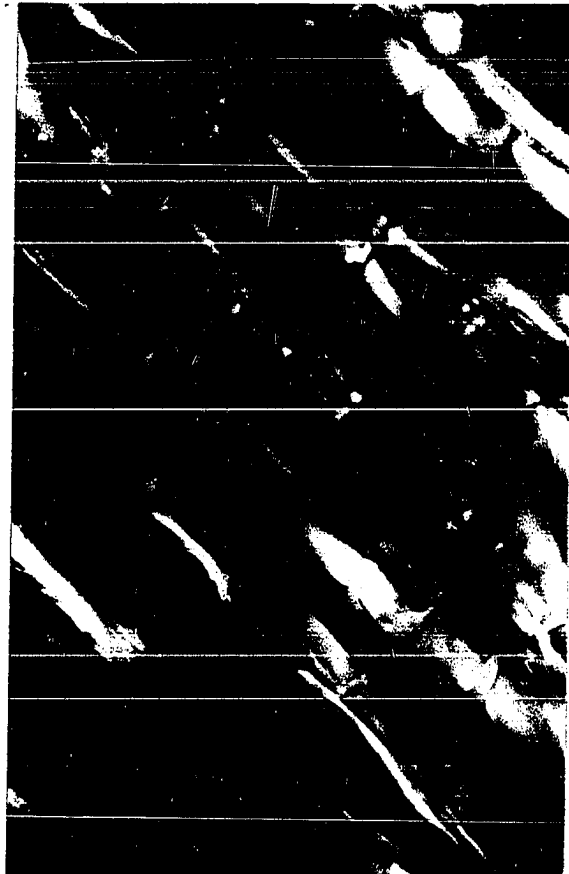servations made with either the electron or polarizing microscopes.

Figure 10. Libriform fibers of the non-leaning tree in polarized
light. Section angle 62.4°, 1000X

Liese (1965) reports, however, that it is present in all species studied

so far in Aceraceae and is present in tension wood cells.

The results of the current study agree with the findings of Wardrop

and Dadswell (1955), i.e., that there is more than one layering sequence

in a species. The layering sequence of the 20° tree was S_1, S_2, S_3, G.

The G layer was relatively thick (Table 1) and was nearly always at least

partially separated from the rest of the cell wall in spite of the care

taken in cutting the embedded specimens. In contrast, the gelatinous

fibers of the 10° tree had no S_3 layer, and the G layer was thin and

usually remained in place in embedded specimens. In fact, at magnifica-

tions below 1000X in unpolarized light, the gelatinous fibers of the 10°

tree could not be distinguished from non-gelatinous ones.

The small number of layer thickness measurements available from the

electronmicrographs indicate that the primary + S_1 and S_3 layer thick-

nesses of Tables 1 and 2 are probably too great. The true values are

probably closer to those presented in the literature review.

At the 99 percent confidence level, the gelatinous fibers of the 10°

tree had a thinner P + S_1 layer (0.41 micron) than did the cells of the

non-leaning tree (0.51 micron). The S_2 layer was thicker (1.74 microns

as compared with 1.40 microns) and the S_3 layer was missing. The G layer

measured only 0.78 micron. The layers of the non-gelatinous fibers were

all significantly thinner than the corresponding layers of the non-lean-

ing tree: the P + S_1 was 0.32 micron as compared with 0.51 micron; the

S_2 was 1.06 microns as compared with 1.40 microns; and the S_3 was 0.34

micron as compared with 0.48 micron.

In the 20° tree, the $P + S_1$ of the gelatinous fibers (0.50 micron) were similar to the same layer of cells of the non-leaning tree (0.51 micron). Both the S_2 layer (1.01 microns) and the S_3 layer (0.31 micron) were thinner than the corresponding layers of the non-leaning tree (1.40 microns and 0.49 micron, respectively). The G layer (1.40 microns) was almost twice as thick as that of the 10° tree. In the non-gelatinous fibers the $P + S_1$ layer (0.45 micron) was not significantly thinner than that of the cells of the non-leaning tree, nor was the S_2 layer (1.42 microns) any different. The S_3 layer was thinner (0.34 micron) than the corresponding layer of the non-leaning tree.

In general then, the $P + S_1$ layers of the leaning trees were as thin or thinner than that of the non-leaning tree. The S_2 layer thickness is commonly variable and such is the case here with no patterns apparent. The S_3 layers of the leaning trees, when present, were always significantly thinner than that of the non-leaning tree.

In total wall thickness, the gelatinous fibers were significantly thicker than the other cells. There was, however, no difference in wall thickness between gelatinous fibers of the 10° tree (2.93 microns) and those of the 20° tree (3.22 microns). The thick S_2 layer of the cells of the 10° tree balanced the thin G layer and the lack of an S_3.

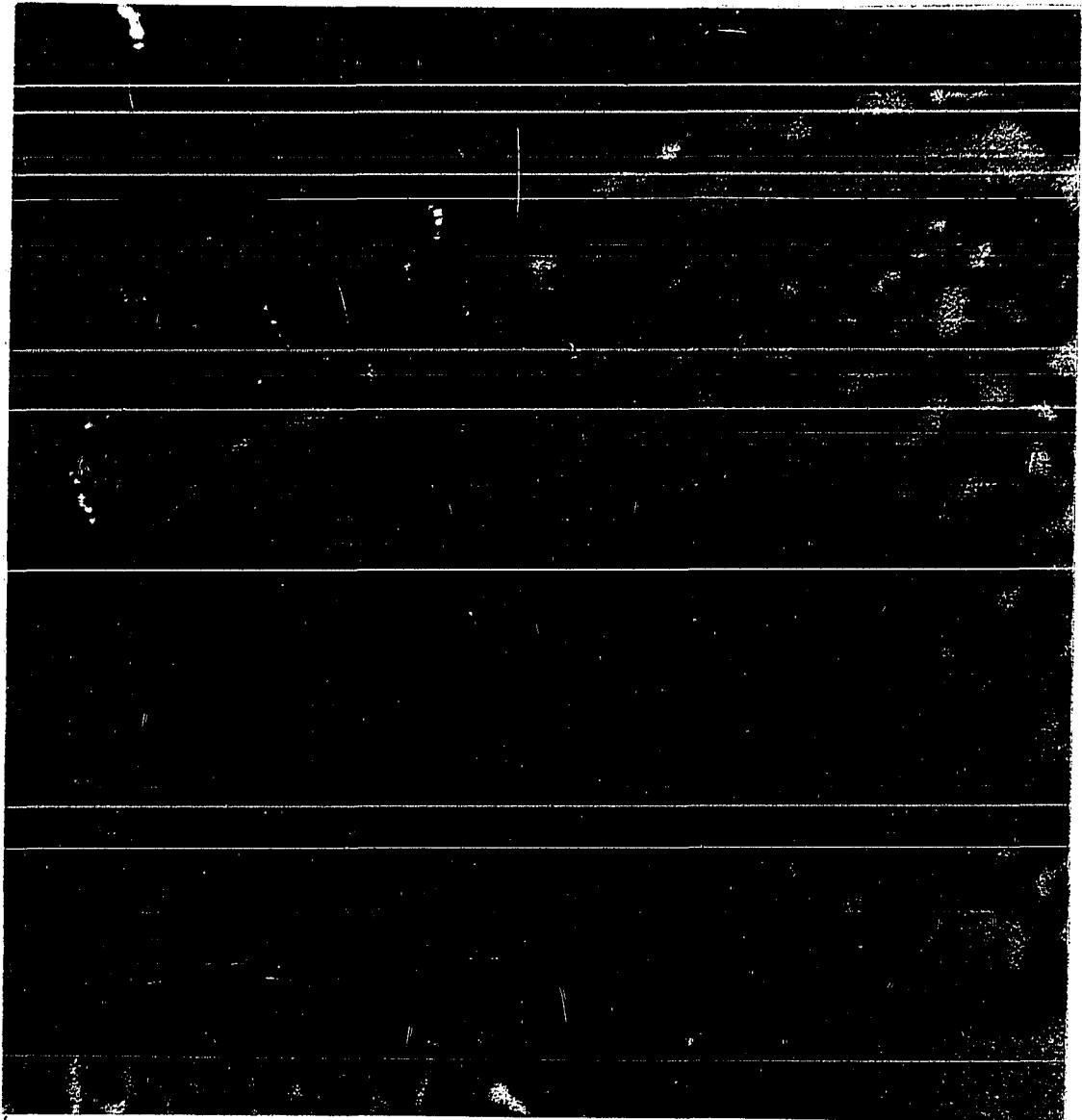Birefringence determinations were made on the two radial walls of

36

Figure 11. Transverse section of portion of gelatinous fiber from tree of 20° lean. Terminating layer and honeycomb structure of G layer visible. Green specimen. Embedded in methacrylate (28,000X)

Figure 12. Longitudinal section of G layer from tree of 10° lean.
Green specimen. Embedded in methacrylate (28,000)

Table 1. Layer thicknesses[1] in the cell radial wall of early wood of three silver maple trees

Layer	Non-leaning tree, normal fibers, microns	Tree of 10° lean		Tree of 20° lean	
		Gelatinous fibers, microns	Non-Gelatinous fibers, microns	Gelatinous fibers, microns	Non-Gelatinous fibers, microns
Primary + S_1	0.51	0.41	0.32	0.50	0.45
S_2	1.40	1.74	1.06	1.01	1.42
S_3	0.48	----	0.34	0.31	0.34
G	----	0.78	----	1.40	----
Total	2.39	2.93	1.72	3.22	2.21

[1]Each value is the average of one measurement on each of 20 cells.

Table 2. Comparison[a] of layer thicknesses in cell radial walls

Primary + S_1 layer

Cell type[b]	$10°$, NG	$10°$, G	$20°$, NG	$20°$, G	$0°$
Thickness, microns	0.32	0.41	0.45	0.50	0.51

S_2 layer

Cell type[b]	$20°$, G	$10°$, NG	$0°$	$20°$, NG	$10°$, G
Thickness, microns	1.01	1.06	1.40	1.42	1.74

S_3 layer

Cell type[b]	$20°$, G	$10°$, NG	$20°$, NG	$0°$
Thickness, microns	0.31	0.34	0.34	0.48

G layer

Cell type[b]	$10°$, G	$20°$, G
Thickness, microns	0.78	1.40

Total wall

Cell type[b]	$10°$, NG	$20°$, NG	$0°$	$10°$, G	$20°$, G
Thickness, microns	1.72	2.21	2.39	2.93	3.22

[a]Duncan's (1955) multiple range test. Any two values not joined by a line are significantly different at the 99-percent confidence level.

[b]$0°$, $10°$, or $20°$ indicates degree of tree lean at breast height; G indicates gelatinous fibers, and NG non-gelatinous fibers from the reaction zone.

fibers from the non-leaning tree to ascertain what the helical winding directions were in the individual wall layers (Figures 13 and 14). The curve for the S_2 layer has a peak at approximately 12° in the wall nearest the observer (Figure 14) but none in the rear wall (Figure 13), indicating a Z helical arrangement of the microfibrils.

The curve for the S_1 layer has a peak at about 44° in the near radial wall, and the S_3 layer has a peak at approximately 20° (Figure 14). Each curve again has a peak in the rear radial wall (Figure 13), the S_1 at about 38° and the S_3 somewhere between 0 and 18°. Peaks in the curves for both walls indicate that the S_1 and S_3 layers have a crossed fibrillar arrangement of both S and Z helices, as has been proven by other investigators using other methods.

The G layer proved to have a Z helix also. Therefore, all sub-sequent birefringence measurements were made only on the radial wall nearest the observer (the left radial wall when facing the bark from the pith). Figures 14 - 18 show the birefringence curves for the secondary cell wall layers of the cell types measured in the three trees. Each point is the average of one measurement on each of 20 cells.

To obtain the fibril angle, the second degree polynominal, $Y = B_0 + B_1X + B_2X^2$, was fitted by the method of least squares regression (Snedecor, 1956) to a part of the range of birefringence observations, Y_i, and associated section angle X_i, for each curve. The maximum point on this fitted quadratic function was then determined by differentiation with respect to X. When the derivative, $\frac{dy}{dx} = 0 + B_1 + 2B_2$, is set equal to

Figure 13. Birefringence plotted against section angle for cell wall layers
of rear radial wall of non-leaning tree. Each point represents
the average of one observation on each of 20 cells

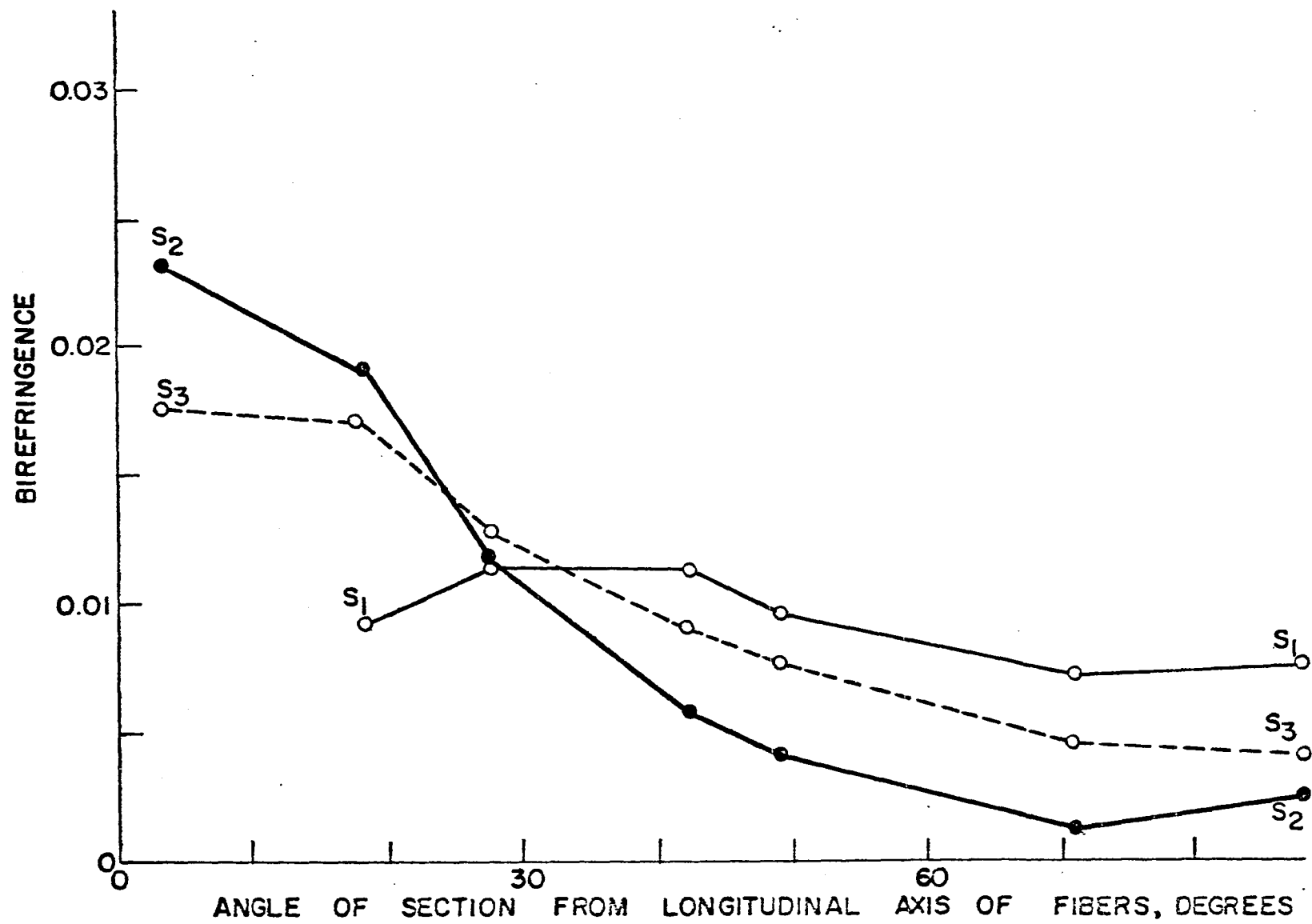Figure 14. Birefringence plotted against section angle for cell wall layers
of radial wall nearest observer of non-leaning tree. Each point
represents the average of one observation on each of 20 cells

Figure 15. Tree of 10° lean, gelatinous fibers. Birefringence plotted against section angle for cell radial wall layers. Each point represents the average of one observation on each of 20 cells
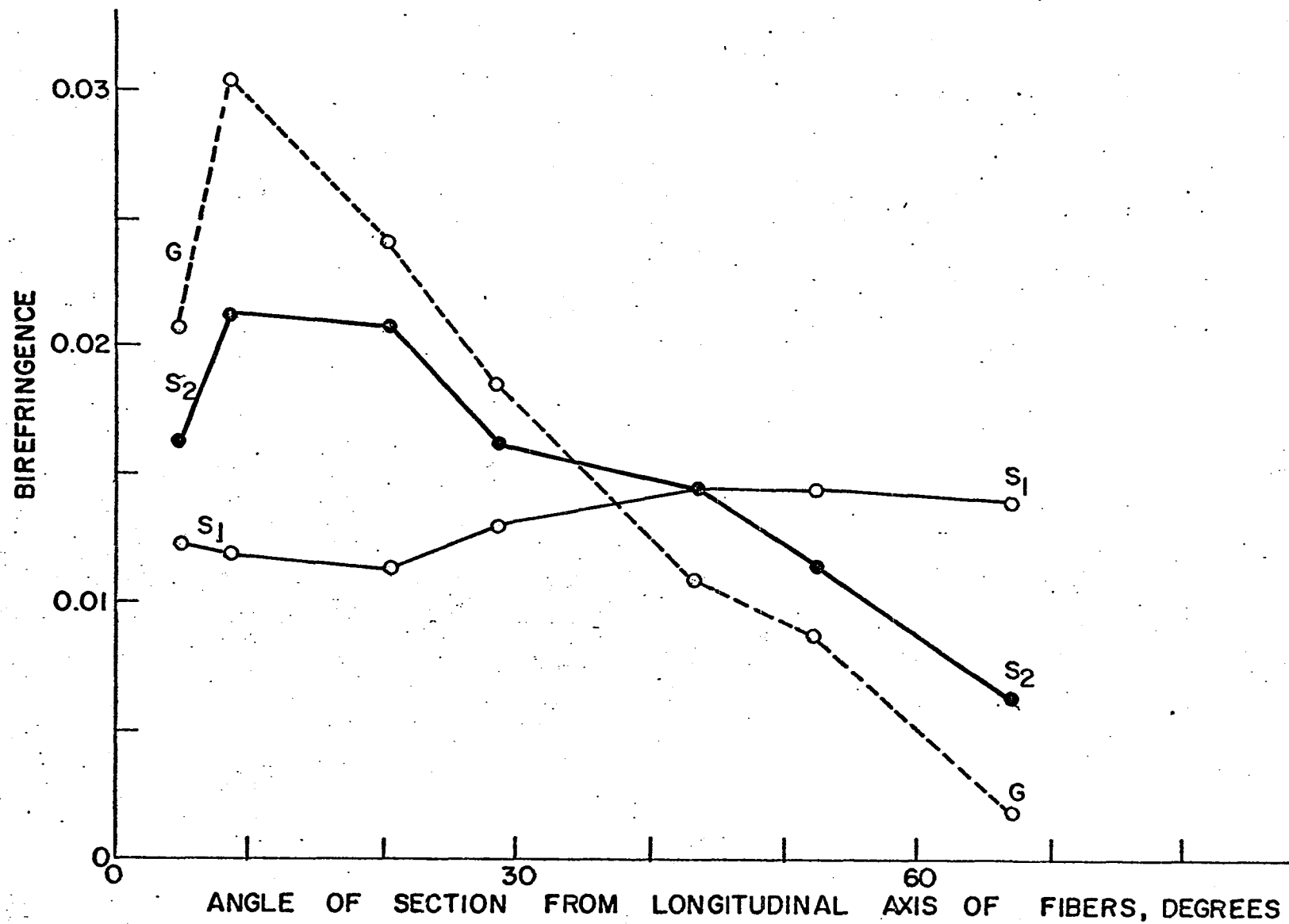
Figure 16. Tree of 10° lean, non-gelatinous fibers. Birefringence plotted against section angle for cell radial wall layers. Each point represents the average of one observation on each of 20 cells

Figure 17. Tree of 20° lean, gelatinous fibers. Birefringence plotted against section angle for cell radial wall layers. Each point represents the average of one observation on each of 20 cells
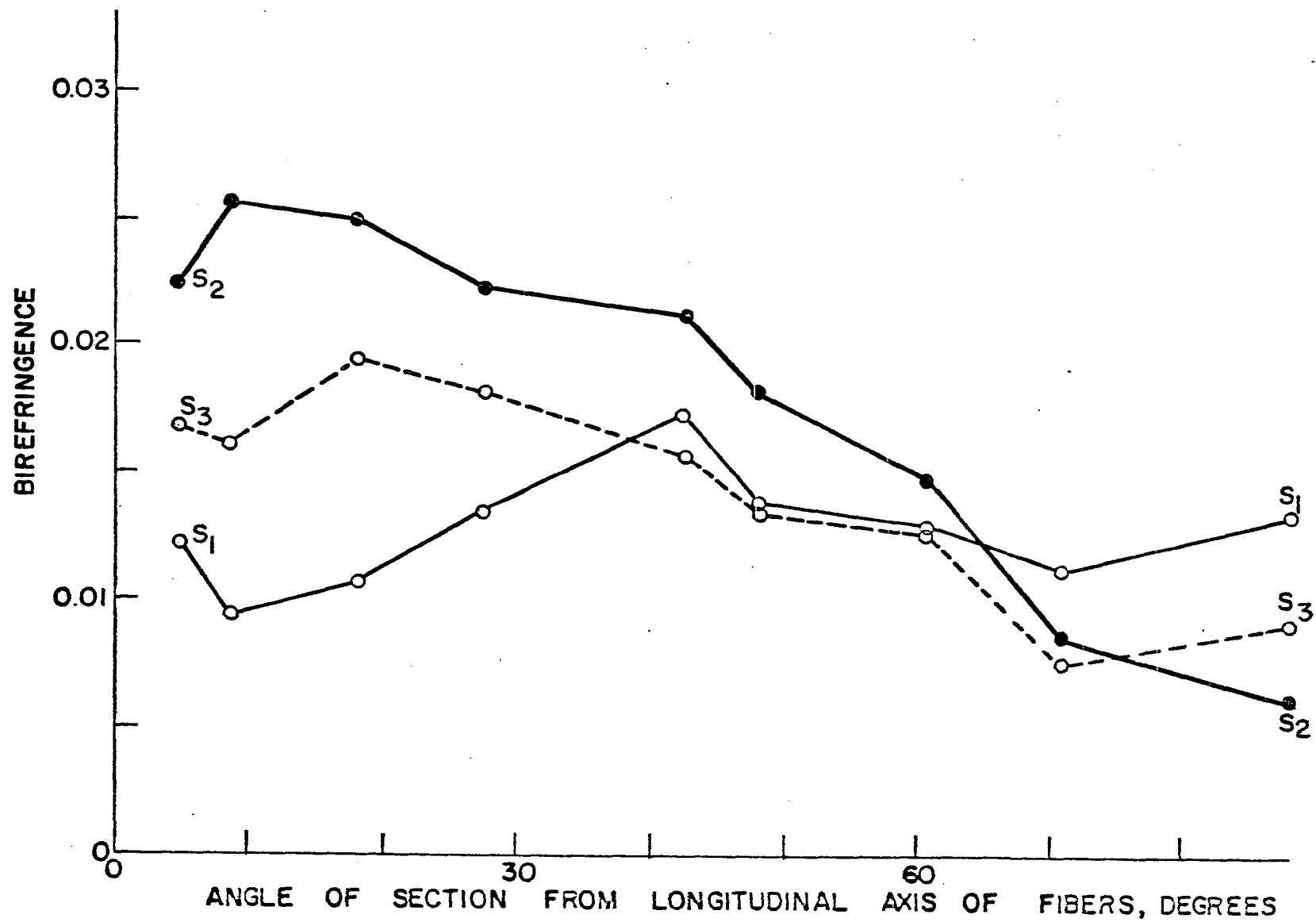
Figure 18. Tree of 20° lean, non-gelatinous fibers. Birefringence plotted against section angle for cell radial wall layers. Each point represents the average of one observation on each of 20 cells
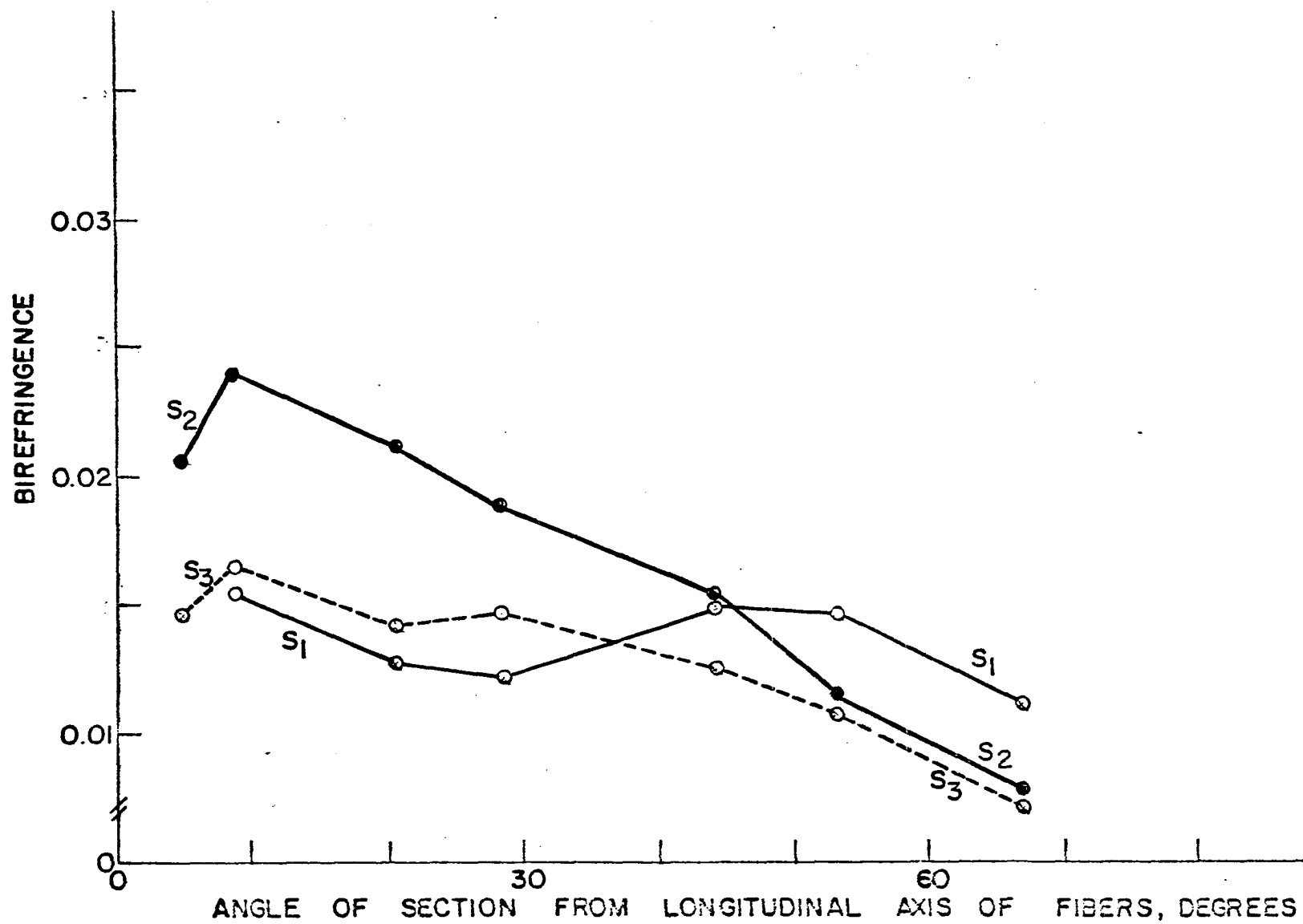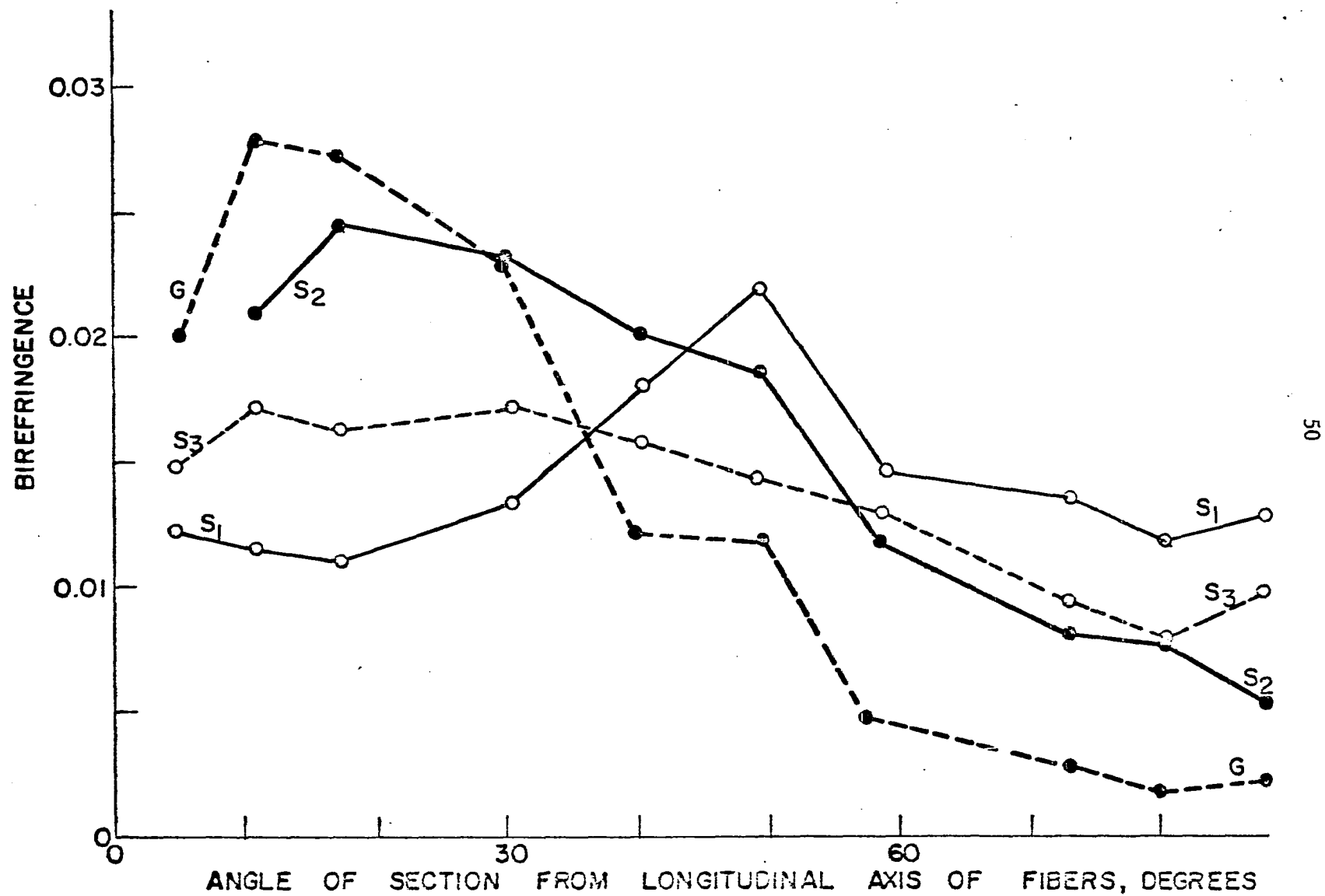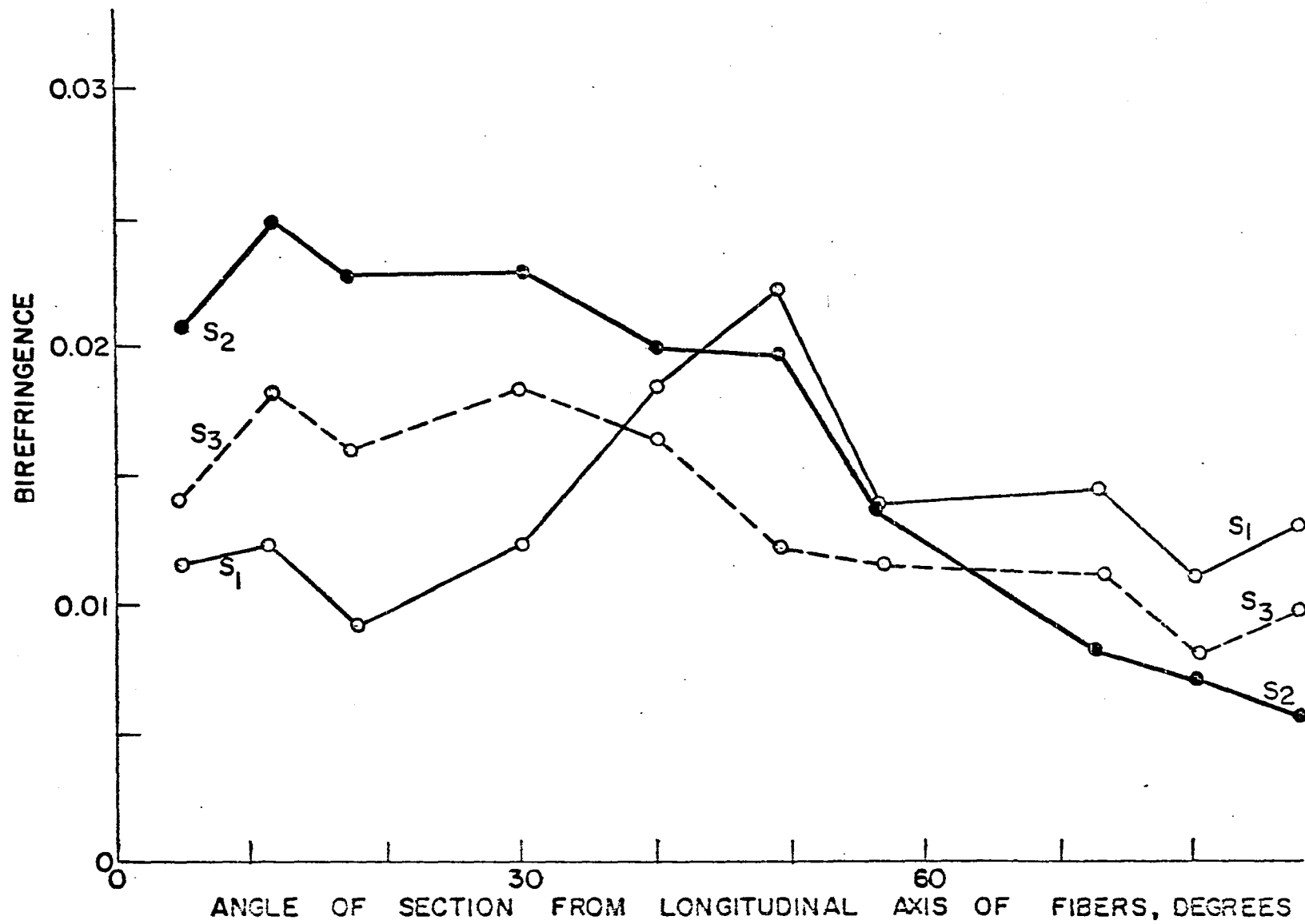
Table 3. Calculated[a] fibril angles in layers of cell radial walls

Layer	non-leaning tree (normal fibers)		
	No. of points[b] n	Range of X[c] degrees	Fibril angle[d] degrees
S_1	7	9-71	44 ± 8
S_2	7	4-61	12 ± 22
S_3	7	9-71	20 ± 24

tree leaning 10 degrees

	Gelatinous fibers			Non-gelatinous fibers		
	No. of points[b] n	Range of X[c] degrees	Fibril angle[d] degrees	No. of points[b] n	Range of X[c] degrees	Fibril angle[d] degrees
S_1	5	20-66	45 ± 3	4	29-66	45 ± 2
S_2	7	5-66	12 ± 33	5	5-43	5 ± 100
S_3	5	20-66	----	5	20-66	29 ± 3
G	5	5-43	8 ± 89	----	-----	-----

tree leaning 20 degrees

	Gelatinous fibers			Non-gelatinous fibers		
	No. of points[b] n	Range of X[c] degrees	Fibril angle[d] degrees	No. of points[b] n	Range of X[c] degrees	Fibril angle[d] degrees
S_1	7	17-80	49 ± 10	7	17-80	51 ± 9
S_2	6	12-58	25 ± 11	10	5-86	11 ± 25
S_3	7	17-80	26 ± 13	5	17-58	29 ± 16
G	7	5-58	15 ± 34	----	----	-----

[a]Based on the second degree polynomial fitted by least squares regression (Snedecor, 1956) to the quadratic portion of the data.

[b]The number of points, n, over which the polynomial is fitted.

[c]The range of X (to the nearest degree) over which the polynomial is fitted.

[d]95% confidence limits.

zero and solved for X, the fibril angle is obtained (Table 3).

The plotted data for the S_1 and S_3 layers (Figures 14 - 18) usually had a relatively smooth form with the major maximum inflection point near the center of the range of X. A second maximum was present between 0 and 12° for each layer. What causes this is unclear; it may be a reflection of the transition zone between the S_1 and S_2 layers and between the S_2 and S_3.

Clearly a second-degree polynomial could not be expected to fit well where more than one inflection point is involved within the range of X. However, where it would fit well, it would be easy to estimate the fibril angle and to construct confidence limits for that estimate, something that previously had not been attempted. The theory appropriate for placing a confidence interval on the point of maximum on a second degree polynomial has been explained by Fuller (1962). Consequently, to use this simple polynomial rather than one of higher degree, it was decided, on the basis of this non-statistical argument, to fit data for only those parts of the range of X which obviously included the maximum and where the second degree equation could be expected to fit adequately. The ranges of X and number of points, n, over which the polynomial was fitted for each layer are given in Table 3.

Under these assumptions Fuller's (1962) method was used to calculate a confidence limit for the true fibril angle, X_{max}. The interval, at 95-percent confidence coefficient is:

$$\frac{B_1 - t_{0.05,n-3} \sqrt{s^2 D(X'X)^{-1}D'}}{2B_2} \leq X_{max} \leq \frac{B_1 + t_{0.05,n-3} \sqrt{s^2 D(X'X)^{-1}D'}}{2B_2}$$

where $t_{0.05,n-3}$ = value of student's t for 95-percent confidence coefficient and n-3 degrees of freedom

s^2 = residual mean square about regression

B_1 = partial regression coefficient for X

B_2 = partial regression coefficient for X^2

D = a 1 x 3 matrix of the terms in $\frac{dy}{dx} = (0 \ B_1 \ 2B_2)$

D' = transpose of D

X = an n x 3 matrix of observations of X_1 with the first row being $(1 \ X_1 \ X_1^2)$ for observation set 1

X' = transpose of X

$(X'X)^{-1}$ = inverse of the (X'X) matrix, i.e., the inverse of the matrix of sum of squares and products of X uncorrected for the means.

The attempt to place confidence limits on the fibril angles was not successful. The points in the quadratic portion of the curves were too few and in the case of the S_2 and G layers, were improperly positioned for the quadratic form to adequately fit. The small number of points resulted in a poor estimate of s^2 and in a small number for the degrees of freedom with a large t value. The data for the S_2 and G layers indicated a steep curve, but the points were too few to define it well. The distribution also was quite unbalanced, with only one point past the maximum. Many of the confidence intervals obtained (66° for the S_2 layer of the gelatinous fibers of the 10° tree, for example) were too wide to be reasonable. This kind of variability is not indicated by the fibril angle values obtained in this study or in other observations made on tension wood.

The fibril angles of the S_1, S_2, and S_3 layers of both gelatinous and non-gelatinous fibers of the leaning trees, with one exception, were similar to or greater than the corresponding angles for the cells of the non-leaning tree. The fibril angles of the 20° tree were generally larger than the corresponding angles of the 10° tree.

In the 10° tree, the S_1 and S_2 fibril angles (45° and 12°, respectively) of the gelatinous fibers were the same as those of the cells of the non-leaning tree. The S_3 layer was missing in the gelatinous fibers. The G layer had a fibril angle of 8°, comparable to the 5 to 8° reported by Wardrop and Dadswell (1948). In the non-gelatinous fibers, the S_1 again had the same fibril angle (45°) as did the cells of the non-leaning tree. The S_2 fibril angle, however, was steep (5°). The S_3 fibril angle was greater (29°) than the 20° of the S_3 layer in cells of the non-leaning tree.

In the 20° tree the S_1 fibril angles for the gelatinous and non-gelatinous fibers were 49° and 51° respectively, as compared to 44° for the S_1 of the non-leaning tree. The gelatinous fiber S_2 layer had a large fibril angle (25°) while that of the non-gelatinous fibers (11°) was similar to the S_1 layer of cells of the non-leaning tree (12°). The S_3 layers of the gelatinous and non-gelatinous fibers (26° and 29° respectively) were again larger than the 20 of the cells of the non-leaning tree. The G layer had a fibril angle of 15°.

DISCUSSION

As explained earlier, shrinkage normally occurs at right angles to the length of the microfibrils during drying. Tension wood exhibits abnormal longitudinal shrinkage which increases as the concentration of gelatinous fibers increases. The results of this study indicate that not only are there greater numbers of abnormal fibers at the greater lean, but that the individual fiber is more prone to longitudinal shrinkage.

In the 10° tree fibril angles and layer thicknesses are not the explanation for abnormal shrinkage. In this tree the fibril angles of the layers present in the gelatinous fibers were similar to those of normal cells. Any component of longitudinal shrinkage normally attributed to the S_1 and S_3 layers would be reduced in these fibers because the $P +$ S_1 layer was thinner than normal and the S_3 was missing. The S_2 layer, which restrains longitudinal shrinkage, was reinforced by its greater thickness and by the G layer, which seemed to be better attached to the rest of the wall than is usual.

The gelatinous fibers of the 20° tree, however, would have increased longitudinal shrinkage if the G layer were assumed not to be attached to the rest of the wall during drying. The fibril angles of the S_1 and the thinner S_3 layers were greater than those of the normal fibers and, more important, the fibril angle of the thick S_2 layer was 25°, as contrasted with 12° for the S_2 of the normal fibers. However, it is doubtful that the results obtained here would explain the 5- to 10-fold increase in longitudinal shrinkage caused by tension wood. The 27° fibril angle of

the S_2 layer is still within the range reported for the S_2 of normal fibers, and the modifications of the other wall layers are not that great.

The explanation for the shrinkage of tension wood is probably similar to that hypothesized by Wardrop and Dadswell (1948, 1955) and Dadswell and Wardrop (1956) to explain irreversible collapse. Lignin is less hydrophylic than cellulose, and lignification is therefore a natural process of dimensional stabilization. Lignin makes direct hydrogen bonding difficult between the cellulose and associated polysaccharides of adjacent microfibrils. In the unlignified G layer, however, the hydroxyl-rich cellulosic surfaces may be able to come into contact on drying with the development of stable hydrogen bonds within the G layer and between it and the adjacent wall layer. As the water is removed from the paracrystalline sheath with its low degree of order, there would be a large shrinkage component in the longitudinal direction. The stress set up could cause the crystalline core to buckle, forcing the entire cell to shrink longitudinally more than normal. Since the remainder of the secondary wall is often reduced or lacking in lignin, this would intensify the effect. This is consistent with the high longitudinal shrinkage of low lignin-containing textile fibers. Sachsse (1962, 1963) found that his air- and oven-dried specimens were compact and did not show the honeycomb structure of the green specimens when the methacrylate was removed. This would indicate that internal bonding had occurred.

The measurement of fibril angles by Senarmont compensation meets a need not now met by either light or electron microscopy. Current techniques of light microscopy permit the determination of the S_2 layer

fibril angle only. Measurements are made of the orientation of bordered pit apertures or of checks produced in the wall by drying stresses. Both follow the orientation of the microfibrils of the thick S_2 layer. In electron microscopy, the orientation of the microfibrils can be observed directly but sections of the individual layers of large numbers of cells cannot be obtained. With senarmont compensation the determination of fibril angles of the individual layers may be based on measurements from large numbers of cells and a statistical approach used for comparisons.

Fuller's (1962) method is the only one presently available for placing confidence limits on the true value of X(fibril angle here) rather than on the value of Y as is normally done. The approach worked very well for several of the S_1 and S_3 curves with the narrowest 95 percent confidence limit being $\pm 2^o$. Wide confidence limits were obtained for many of the curves but this was caused by insufficient data. More points located on both sides of the maximum in the quadratic portion of the curve would define curves which fit the data more closely and would increase the degrees of freedom.

The anatomical changes observed in the trees of increasing lean do not fully explain abnormal shrinkage of tension wood. With the Senarmont compensation method now developed, more trees should be sampled to determine whether the results obtained here truly represent typical leaning trees. Further research is necessary in the chemical composition and bonding of the wall layers of the reaction wood tissue.

More research is needed in the physical and chemical nature of the G layer and in the nature of its attachment to the rest of the cell wall.

The apparent honeycomb structure and loose texture of the G layer is based on data collected from methacrylate-embedded material. The methacrylate swells the G layer but not the rest of the wall during polymerization. The observations are therefore made on specimens subjected to very disruptive forces and should be verified by specimens embedded in Epon and etched or on replicas.

SUMMARY

Mature wood in three silver maple trees leaning 0°, 10°, and 20°

from the vertical was compared in cell radial wall layering sequence,

thickness and fibril angle. Observations were made under a polarizing

microscope which was equipped with a Senarmont compensator for the

fibril angle determinations. An attempt was made for the first time,

to place confidence limits on the fibril angles obtained. The results

indicate that the method will work well if more data are taken for the

quadratic portion of the birefringence curves.

Longitudinal shrinkage increases with increase of lean and with

increase in percent of gelatinous fibers. The results obtained from

the tree of 10° lean (18% gelatinous fibers) would not explain increased

longitudinal shrinkage. The S_3 layer was absent in the gelatinous fibers.

The S_2 layer, which usually controls shrinkage, had a fibril angle similar

to that of cells from the non-leaning tree and it was thicker. The P

+ S_1 layer was thin with a fibril angle similar to that of normal cells.

The G layer was thin, well attached to the rest of the wall, and had a

steep fibril angle (8°). The non-gelatinous fibers had thinner P +

S_1, S_2, and S_3 layers than did cells of the non-leaning tree, while the

fibril angle of the S_1 was similar, that of the S_2 was smaller, and that

of the S_3 was greater than normal.

The results obtained from the 20° tree (48.5 percent gelatinous

fibers) would indicate increased longitudinal shrinkage, but not of

the magnitude found associated with large concentrations of tension

wood. The gelatinous fibers contained a thick, poorly attached G layer
(fibril angle of 15°) in addition to the usual cell wall layers. In
both gelatinous and non-gelatinous fibers the fibril angles of the layers
tended to be larger than those of cells from the non-leaning tree, es-
pecially the S_2 layer (25°) of the gelatinous fibers. In thickness, the
cells of the 20° tree differed from those of the non-leaning tree only
in that the S_2 layer of the gelatinous fibers was thinner and both gel-
atinous and non-gelatinous fibers had a thinner S_3 layer.

Electron micrographs indicate that the G layer had the typical
honeycomb structure and terminating layer observed when swollen by
methacrylate. Investigations should be performed on the undisturbed
material using other embedding media and techniques to determine whether
this is artifact.

LITERATURE CITED

Arganbright, Donald G. 1964. The occurrence and shrinkage characteristics of tension wood in soft maple. Unpublished M.S. thesis. Ames, Iowa, Library, Iowa State University of Science and Technology.

Barefoot, A. C. 1963. Selected wood characteristics of young yellow-poplar. 2. Shrinkage of normal and abnormal wood. For. Prod. J. 13: 443-448.

Baudendistel, M. E. and V. Akins. 1946. High longitudinal shrinkage and gelatinous fibers in an eccentric cottonwood log. J. For. 44: 1053-1057.

Berlyn, G. P. 1961. Factors affecting the incidence of reaction tissue in Populus deltoides Bartr. Iowa State J. Sci. 35: 367-424.

Brendemuehl, R. H., A. L. McComb, and G. W. Thomson. 1961. Stand yield and growth of silver maple in Iowa. Iowa State University of Science and Technology Cooperative Extension Service in Agr. and H. Ec. Pamphlet F-159.

Carlson, T. C. ca. 1964. Preparing wood sections for measurement of cellular dimensions. Unpublished Mimeograph Princeton, West Virginia, Forest Products Marketing Lab.

Carl Zeiss Optical Co. ca. 1956. Directions for using the Senarmont-compensator. Unpublished multigraph. Oberkochen/Württ., Germany, Carl Zeiss Optical Co.

Casperson, C. 1961. Über die Bildung von Zellwanden bei Laubholzern. 2. Mitteilung. Der Zeitliche Ablauf der Sekundärwandibldung. Zeitschrift für Botanik 49: 289-306.

Chow, K. Y. 1946. A comparative study of the structure and chemical composition of tension wood and normal wood in Beech (Fagus sylvatica L.). Forestry 20: 62-76.

Clarke, S. H. 1937. The distribution, structure, and properties of tension wood in Beech (Fagus sylvatica L.). Forestry 11: 85-91.

Cockrell, R. A. 1946. Influence of fibril angle on longitudinal shrinkage of ponderosa pine wood. J. For. 44: 876-878.

Côté, W. A., Jr. and A. C. Day. 1962. The G layer in gelatinous fibers-electron microscopic studies. For. Prod. J. 12: 333-338.

Dadswell, H. E. and A. B. Wardrop. 1949. What is reaction wood? Aust. For. 13: 22-23.

Dadswell, H. E. and A. B. Wardrop. 1956. The importance of tension wood in timber utilization. Proc. Aust. Pulp and Paper Ind. Tech. Assoc. 10: 30-42.

Duncan, D. B. 1955. Multiple range and multiple F tests. Biometrics 11: 1-42.

Fuller, W. A. 1962. Estimating the reliability of quantities derived from empirical production functions. J. Farm Econ. 44: 82-99.

Hodge, A. J. and A. B. Wardrop. 1950. An electron microscopic investigation on the cell wall organization of conifer tracheids. Nature 165: 272-275.

Johannsen, A. 1918. Manual of petrographic methods. 2nd ed. New York, New York, McGraw-Hill Co.

Jutte, S. M. 1956. Tension wood in Wane (Ocotea rubra Mez.). Holzforschung 10: 33-35.

Koehler, A. 1960. Longitudinal shrinkage of wood. U.S. Dept. Agr. For. Prod. Lab. Rept. 1093.

Liese, Walter. 1965. The warty layer. In Côté, W. A., Jr., ed. Cellular ultrastructure of woody plants. pp. 251-270. Syracuse, New York, Syracuse University Press.

Mühlethaler, Kurt. 1965. The fine structure of the cellulose microfibril. In Côté, W. A., Jr., ed. Cellular ultrastructure of woody plants. pp. 191-198. Syracuse, New York, Syracuse University Press.

Ollinmaa, P. J. 1956. On the anatomic structure and properties of tension wood in birch. Acta Forestalia Fennica 64: 171-263.

Onaka, F. 1949. Studies on compression and tension wood. Kyoto Wood Res. Inst. Bull. 1.

Panshin, A. J., Carl De Zeeuw, and H. P. Brown. 1964. Textbook of wood technology. Vol. 1 2nd ed. New York, New York, McGraw-Hill Book Co.

Peck, E. C. 1957. How wood shrinks and swells. For. Prod. J. 7: 235-244.

Pillow, M. Y. 1950. Presence of tension wood in mahogany in relation to longitudinal shrinkage. U.S. Dept. Agr. For. Prod. Lab. Rept. D1763.

Preston, R. D. 1951. Fibrillar units in the structure of native cellulose. Faraday Soc. Disc. 11: 165-170.

Preston, R. D. 1952. The molecular architecture of plant cell walls. New York, New York, John Wiley and Sons, Inc.

Preston, R. D. and V. Ranganathan. 1947. The fine structure of the fibers of normal and tension wood in Beech (Fagus sylvatica L.) as revealed by X-rays. Forestry 21: 92-98.

Rendle, B. J. 1937. Gelatinous wood fibers. Tropical Woods 52: 11-19.

Sachsse, Hanno. 1962. Electronemikroskopische Untersuchungen über die Zellwandstruktur von Zugholzfasern. Holz als Roh- und Werkstoff 20: 429-433.

Sachsse, Hanno. 1963. Der Submikroscopische Bau der Faserzellwand beim Zugholz der Pappel. Proc. Section 41, Internat. Union For. Res. Organ.

Sass, John E. 1958. Botanical microtechnique. 3rd ed. Ames, Iowa, Iowa State University Press.

Snedecor, George W. 1956. Statistical methods. Ames, Iowa, Iowa State University Press.

Terrell, B. Z. 1952. Distribution of tension wood and its relation to longitudinal shrinkage in aspen. U.S. Dept. Agr. For. Prod. Lab. Rept. R1917.

U.S. Forest Service. 1965. Silvics of forest trees of the United States. U.S. Dept. Agr. Handbook 271.

Wahlgren, H. E. 1957. Tension wood in overcup oak. U.S. Dept. Agr. For. Prod. Lab. Rept. 2089.

Wahlstrom, E. E. 1960. Optical crystallography. 3rd ed. New York, New York, John Wiley and Sons, Inc.

Wardrop, A. B. 1964. The structure and formation of the cell wall in xylem. In Zimmermann, Martin H., ed. The formation of wood in forest trees. pp. 87-134. New York, New York, Academic Press, Inc.

Wardrop, A. B. and H. E. Dadswell. 1947. Contributions to the study of the cell wall. 5. The occurrence, structure, and properties of certain wall deformations. Australian Council for Sci. Ind. Res. Bull. 221.

Wardrop, A. B. and H. E. Dadswell. 1948. The nature of reactionwood. 1. Structure and properties of tension wood fibers. Aust. J. of Sci. and Res. Series B-1: 3-16.

Wardrop, A. B. and H. E. Dadswell. 1955. The nature of reaction wood. 4. Variations in cell wall organization of tension wood fibers. Aust. J. of Bot. 3: 177-189.

ACKNOWLEDGEMENTS

I would like to express my gratitude to Dr. D. L. Biggs for the use of his polarization facilities and to Dr. C. C. Bowen for my thorough training in electron microscopy.

I am deeply indebted to Dr. D. W. Bensend who has greatly influenced my professional development and who has contributed so much to the development of both the hypotheses and the techniques of this research.

To my wife, Mary, I owe an immeasurable debt for her patience and complete support.

APPENDIX

Mayer's Hemalum Stain (Sass, 1958)

Preparation

1. Dissolve 20 g. potassium alum in 1 l. boiling water.

2. Add 1 g. hematoxylin crystals to the above. Remove from the heat when dissolved.

3. Add 2 g. sodium iodate.

4. The stain is ready for use. Filter whenever a metallic scum is visible on the surface of the stain. The stain gradually disintegrates and should be made up fresh every 2 or 3 weeks.

Staining

1. Section should have been in distilled water.

2. Place section in the stain.

3. Allow to stand 5 to 30 minutes.

4. Place section in distilled water 1 minute.

5. Wash in running tap water 3 to 5 minutes.

Chloriodide of Zinc Stain (Arganbright, 1964)

Preparation

1. Stock solution of zinc chloride.

    Add 432 g. of zinc chloride to 100 cc of distilled water.

2. Potassium iodide solution.

    7 cc of distilled water.

    5 g. of potassium iodide.

0.9 of iodine ground to a fine powder in mortar and pestle.

3. Solution 2 is added to 37 g. of the saturated stock solution

of zinc chloride. This breaks down rapidly in light so the

container should be covered with dark paper or aluminum foil.

Staining

1. Wash the section with water.

2. Flood the section with the stain.

3. Allow to stand 30 seconds.

4. Drain off the stain and add a fresh drop.

5. Add a coverslip and seal with beeswax.

Methacrylate Embedding Schedule

1. Specimen sizes were 80 to 120 microns longitudinally and 0.5

to 1.0 mm. radially and tangentially.

2. Dehydrate stepwise in ethanol.

30%, 50%, 70%, 80%, 95%, absolute ethanol twice--15 minutes each.

3. Place specimen in equal parts of absolute ethanol and the monomer

for 1 hour. The monomer was 8 n-butyl to 2 methyl methacrylate.

4. Place specimen in pure monomer twice, 12 hours each.

5. Place specimen in monomer plus 2% catalyst for 12 hours. The

catalyst is benzoyl peroxide (Luperco CDB). Periodically pull

a vacuum to remove air bubbles.

6. Polymerize in no. 2 gelatin capsules at 50°C. until hard. The

relative proportions of the n-butyl and methyl methacrylates

may be changed to attain a hardness similar to that of the

specimen. Increasing the concentration of the methyl meth-

acrylate increases the polymer hardness.